Evaluating a Wearable Sensor-Based Tibia Force Estimation Algorithm for Applications in Stress Fracture Reduction in Runners

By

Lauren M. Branscombe

Thesis

Submitted to the Faculty of the
Graduate School of Vanderbilt University
in partial fulfillment of the requirements
for the degree of

MASTER OF SCIENCE
in
Mechanical Engineering

May 31, 2018

Nashville, Tennessee

Approved:
Karl E. Zelik, Ph.D.
Thomas J. Withrow, Ph.D.

TABLE OF CONTENTS

Page

LIST OF FIGURES

Figure Page

LIST OF TABLES

Table Page

Chapter 1: Introduction

Section 1.1 Stress Fracture Injuries

Many people run recreationally to stay fit and active, however, suddenly altering one's training regime can result in injury that inhibits continued exercise. Recreational runners in particular are highly prone to developing stress fractures, especially when their form changes or their mileage increases substantially in a short period of time (Harrast & Colonno, 2010). Other at-risk populations include military trainees and some industrial workers who experience high or repetitive loading of the legs (Milgrom et al., 1985). While not as severe as traumatic injuries such as complete bone fractures, these stress fractures are common, comprising up to ten percent of all sports injuries, and can result in significant pain, may prevent a runner from training for weeks or months following injury, and may result in substantial healthcare costs (Matheson et al., 1987). Healing often occurs naturally with 6-8 weeks of rest (i.e., no running) but may also require immobilization of the leg. Runners who experience stress fractures have also been shown to be more susceptible to re-injury, particularly when insufficient recovery time is taken (Diehl, Best, & Kaeding, 2006).

Many important questions about the factors that contribute to the development of a stress fracture remain unanswered, but there are several methods of measuring or estimating lower limb bone loading, including both invasive (i.e., Lanyon, Hampson, Goodship, & Shah, 1975) and non-invasive (i.e., Moissenet, Chèze, & Dumas, 2014) techniques, which may help to provide insight into the mechanisms of this injury. It is hypothesized that non-invasive estimates of bone loading can be used to prospectively study and predict the occurrence of stress fractures by

monitoring a large number of runners over time and finding common trends in loading amongst runners that develop injuries (Milner, Ferber, Pollard, Hamill, & Davis, 2006).

The goal of the present study is to determine if a set of portable, wearable sensors can be used to accurately and reliably estimate tibia bone loading, so that measurements could be taken outside of a laboratory setting. In the short term, this would allow researchers to monitor bone loading trends during an athlete's day to day running regime, as opposed to on a treadmill in a laboratory. Once risk factors are identified, the long term goal is to design a device to monitor bone loading in runners and provide feedback about potentially harmful trends in their loading patterns. This type of device has the potential to warn the user that damage may be accumulating in the bone prior to the onset of symptoms, ultimately reducing the occurrence of stress fractures in the recreational runner population.

Section 1.1.1 Stress Fracture Physiology

Bones experience constant cycles of damage and repair, but in most instances, cells are able to heal themselves before severe damage and noticeable pain occurs. During regular loading of human bones, microcracks form, and the propagation of these cracks is what leads to injury. In healthy bones, these microcracks form and heal without ever resulting in pain or injury. However, it is theorized that stress fracture injury occurs when the rate of crack formation/propagation is greater than the rate of repair. There is some correlation between the presence of microcracks and the ability to repair them; a greater occurrence of microcracks results in an increased rate of bone re-healing, but it has been proposed that this re-healing results in the bone becoming more porous, and thus more susceptible to the formation of new or larger cracks (Martin, Burr, Sharkey, & Fyhrie, 2015). Therefore, during a rapid increase in

activity level, such as at the beginning of training for a long race, or at the beginning of military training, bones may not have enough time to heal sufficiently, resulting in a greater incidence of injury. Scientists generally agree that in order to prevent stress fractures, there must be sufficient healing time between loadings, although exact requirements likely vary from person to person and remain largely unknown (Ghiasi, Chen, Vaziri, Rodriguez, & Nazarian, 2017).

Section 1.1.2 Stress Fractures Causes

While it is known that the propagation of microcracks in a bone leads to stress fractures, it is unclear which characteristics of bone loading are most predictive of injury. Scientists have cited a variety of factors as the source of tibia stress fracture development including impact peak, active peak, loading rate of ground reaction forces or tibia forces, and tibia acceleration or shock, however, some proposed causes have since been shown not to influence injury (Bennell, Matheson, Meeuwisse, & Brukner, 1999). In general, it is assumed that an increase in some combination of peak forces and loading rates on the bone is correlated with the occurrence of stress fractures. Some researchers have also suggested that ground reaction forces, rather than bone forces, can be used to analyze stress fracture risks, though recent studies have shown that there is little correlation between these metrics and injury (Nigg, Mohr, & Nigg, 2017; Worp, Vrielink, & Bredeweg, 2016). Magnitude changes in any of these peak forces or loading rates could be attributed to a change in intrinsic (i.e. muscle activation, running technique, bone properties) or extrinsic (i.e. shoes, terrain) factors associated with a run. Research in this area has been inconclusive, and some groups are now shifting their focus towards the investigation of not just the characteristics of an average loading cycle but also the effects of number of loading cycles or amount of recovery time on the development of tibia stress fractures (Edwards, Taylor,

Rudolphi, Gillette, & Derrick, 2009, 2010). It is proposed that changes in training such as increased mileage per run or increased number of training sessions per week may be more important than changes in one's gait cycle in predicting stress fracture development (Goldberg & Pecora, 1994). To truly understand the causes of stress fractures, we must first have a way to measure bone loading in daily running and identify trends in metrics that are common amongst populations that develop stress fractures.

Section 1.1.3 Common Stress Fracture Injury Sites

In athletes, especially runners, stress fractures are most common in the lower extremities, particularly the foot, heel, and lower leg, with tibia stress fractures being the most common amongst this population (Matheson et al., 1987). Among stress fractures of the tibia, most occur medio-posteriorly and in the upper or lower third of the bone (Orava & Hulkko, 1984). This information may be useful in determining the important loading factors that lead to these injuries (i.e. whether to focus on bending forces or torsion forces). For the purposes of this study, we will focus on measuring tibia bone loading in order to develop a way to analyze tibia stress fracture risks.

Section 1.2 Estimating Tibia Force

Fundamentally, stress fractures are caused by the forces applied to the bone, so finding a reliable way to estimate this loading is a crucial first step to determining any identifiable risk factors prior to injury. Built on the knowledge of the forces applied to the tibia, researchers have developed methods of analytically estimating bone loading from external measurements, which

are treated as "ground truth" in this study. The rationale for trusting this approach is outlined below, and a detailed description of calculations is included in Methods.

Section 1.2.1 Forces Acting on the Tibia

In order to determine bone loading of the tibia, we must understand which forces are acting on the bone, and how to estimate each of these forces. Many forces need to be considered in a full biomechanical analysis of bone loading: gravitational forces due to the mass of each limb segment, external (ground reaction) forces, muscle and ligament forces at each joint, and joint reaction forces due to the interactions between each limb segment (Winter, 2009). In determining the force experienced by the tibia, we measure the forces acting on the foot, and use inverse dynamics to find the forces acting on the tibia at the ankle (Robertson, Caldwell, Hamill, Kamen, & Whittlesey, 2013). It should be noted that some of the force at the ankle is borne by the fibula, though research has shown that over 90% of forces at the ankle act on the tibia (Funk, Rudd, Kerrigan, & Crandall, 2004; Lambert, 1971). It is sometimes thought that ground reaction force is a surrogate for calculating tibia bone loading, yet the ground reaction force has a much lower magnitude than the total force on the bone. As shown in Figure 1, tibia force is indeed influenced by ground reaction force, but also largely by muscle forces, resulting in peak loading that is three to six times peak ground reaction force (Scott & Winter, 1990).

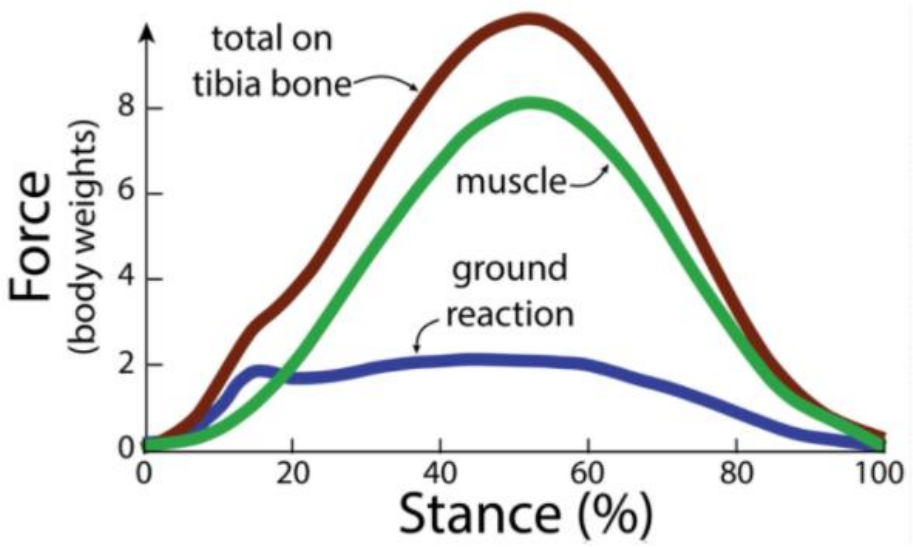

Figure 1. Tibia force during the stance phase of running. Tibia force is composed of ground reaction forces and muscle forces acting on the bone (Scott & Winter, 1990).

Forces acting directly on the tibia, including ankle reaction force, and forces from the Achilles tendon and calf muscles, are influenced by ground reaction force, but summed together, create a much higher load on the bone. Figure 2 illustrates how these forces act at angles with respect to the tibia, yielding compressive forces, shear forces, and bending moment (Scott & Winter, 1990). There are also torsional forces on the bone, which may influence stress fracture development (Yang et al., 2014). For this study, we will isolate compressive loads on the tibia, neglecting shear and torsional components of loading, which are much lower in magnitude. The focus of this study will be on loading near the distal end of the tibia, since this is one of the most common locations of tibia stress fractures in runners. With this the case, we can isolate the distal end of the bone, closest to the ankle, and analyze the forces acting at this position.

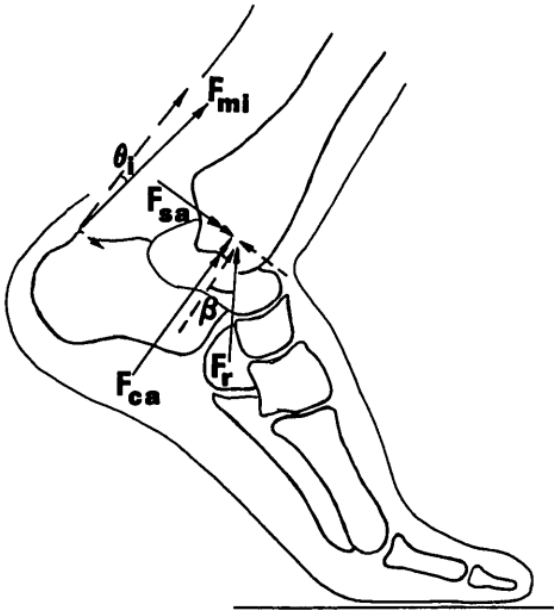

Figure 2. Schematic of forces applied to the distal end of the tibia. F_{mi} represents muscle force, acting at an angle θ_i to the tibia, F_r is the reaction force at the ankle, acting at an angle of β to the tibia, and F_{ca} and F_{sa} are the resultant compressive and shear force vectors acting on the tibia (Scott & Winter, 1990).

At the distal end of the tibia, bone force is equal to the sum of net joint force and forces from muscles, ligaments, and joint contact. This knowledge is derived from first principles of physics, deriving a free body diagram and performing a force balance on the tibia, but also confirmed experimentally through cadaver studies. Sharkey and Hamel conducted a study simulating the stance phase of gait in cadaver feet and measured the forces in each of five actuator systems representing muscle contractions, as well as ground reaction forces and actual tibia compression forces (Sharkey & Hamel, 1998). The results of this study, shown in Figure 3, demonstrate that tibia force is well approximated as the sum of the ground reaction force and muscle contributions; error during mid-stance and at peak tibia loading was within one tenth of a body weight, and error throughout stance remained less than one half of a body weight. This

study confirms that tibia force can be calculated as the sum of forces originating external to the body (from ground reaction forces) and forces originating internal to the body (muscles/tendons).

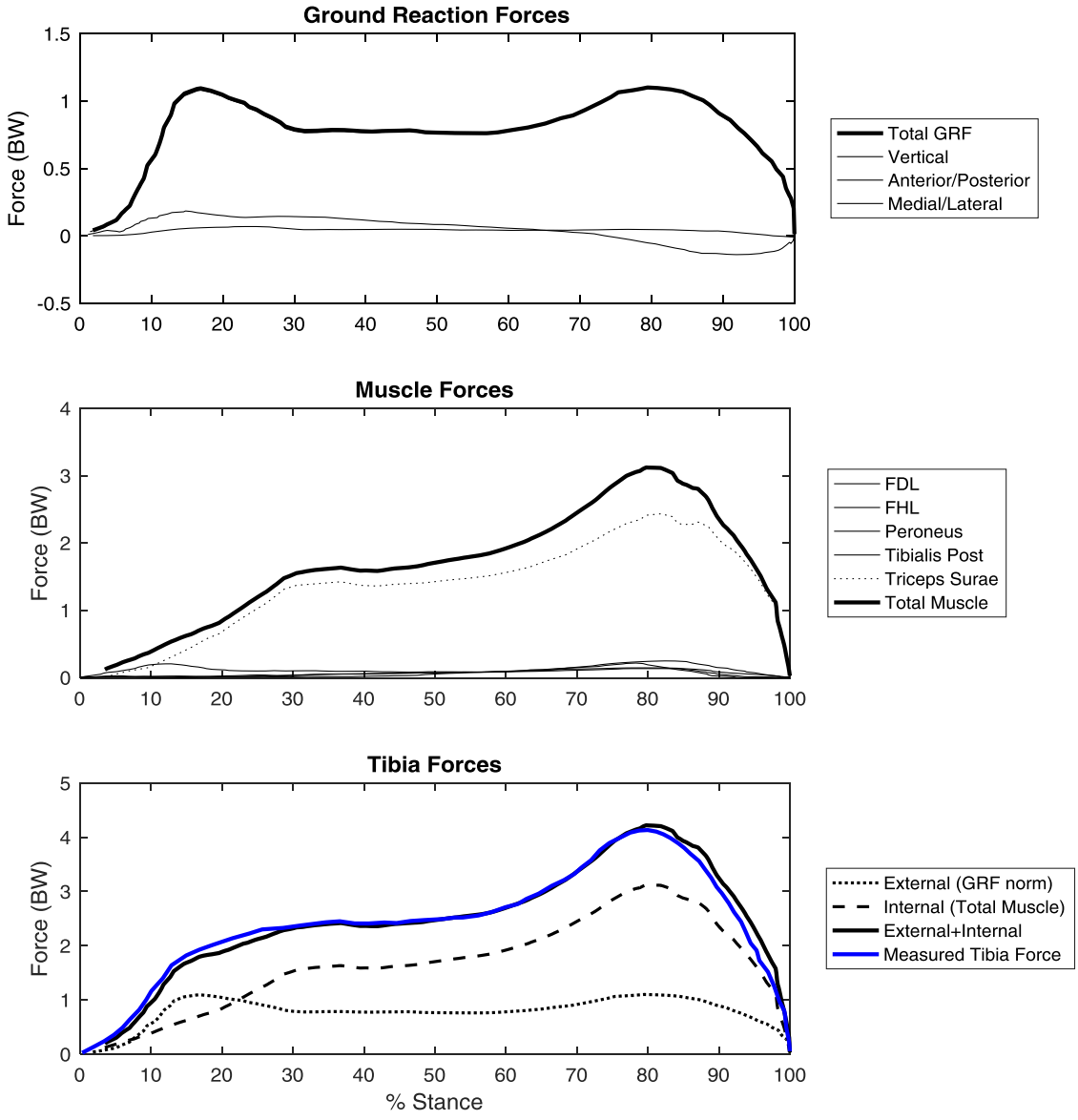

Figure 3. Results from Sharkey et al. showing that tibia force is nearly equal to the sum of ground reaction forces and muscle forces.

Since the mass and acceleration of the foot are small during the stance phase of gait, inertia of the foot is neglected (Siegler, Moskowitz, & Freedman, 1984). Therefore, net joint force at the ankle can be closely approximated by ground reaction force. The compressive component of this force felt by the tibia is determined by projecting the ground reaction force vector onto the axis of the bone. In addition to net ankle force, muscle, ligament, and joint friction and damping forces must be accounted for in order to gain a full understanding of tibia loading. Previous literature has indicated that ligament forces are small in comparison to muscle and joint reaction forces, and that effects of friction and damping at the ankle joint is negligible in healthy subjects (Miller, Esterson, & Shim, 2015; Silder, Heiderscheit, & Thelen, 2008; Steele, Demers, Schwartz, & Delp, 2012). This leaves us with ground reaction forces and muscle forces contributing to tibia force, which, as seen in Figure 3, has been shown to be a close approximation of actual tibia load (Sharkey & Hamel, 1998).

In order to estimate total muscle force applied to the tibia during stance, an inverse dynamics approach will be used, where force is derived from net ankle moment divided by muscle moment arm. In a complete analysis of forces on the tibia, medial/lateral and anterior/posterior moments would be considered, but in running, these contributions are small (Eng & Winter, 1995), and are thus neglected. We instead focus on plantarflexors and dorsiflexors and aim to determine the forces in these muscles during stance. At the ankle, the tibialis anterior acts as a dorsiflexing muscle, but is only active immediately after foot contact. At the beginning of stance when the tibialis anterior is activated, we expect that our estimate of tibia force will be lower than the actual force, which is acceptable, given that tibia loads are relatively low during this portion of stance. We believe that even without estimating the contributions of this dorsiflexing muscle, we will still be able to accurately estimate peak

loading, and since it is not currently believed that this initial phase of stance is important in terms of stress fracture development, we feel comfortable making this simplification (Nigg, 2010; Nigg et al., 2017). Therefore, for most of stance, we can assume there is no force contribution from dorsiflexing muscles, and it is reasonable to neglect co-contraction (Almonroeder, Willson, & Kernozek, 2013; Kernozek, Gheidi, & Ragan, 2017; Sasimontonkul, Bay, & Pavol, 2007).

In addition to assumptions about the contributors to ankle moment, we must also be able to justify the selection of an appropriate muscle moment arm. In reality, each muscle group has a separate and changing moment arm, a function of muscle force and ankle angle (Honert & Zelik, 2016; McCullough, Ringleb, Arai, Kitaoka, & Kaufman, 2011; Silder, Whittington, Heiderscheit, & Thelen, 2007). However, we do not know precisely how the forces that comprise ankle moment are partitioned between muscle groups for an individual subject or task; this is considered a grand challenge in the field of biomechanics. For this study, we will assume a constant moment arm, which is reasonable under the given circumstances. Prior studies have estimated that 90% of muscle force can be attributed to the Achilles tendon and triceps surae muscle group (Bogey, Perry, & Gitter, 2005; Honert & Zelik, 2016). This muscle group shares a common tendon insertion, with a moment arm from the ankle joint of about 5 cm that does not vary substantially over the range of forces or motion in running. Several imaging-based studies estimated changes in moment arm of less than 2 cm across the entire range of motion of the ankle (Maganaris, Baltzopoulos, & Sargeant, 1998; McCullough et al., 2011; Rugg, Gregor, Mandelbaum, & Chiu, 1990). In the case of running, the ankle does not experience full range of motion, so we expect this change in moment arm to be even smaller, and do not anticipate this simplification to confound our results. Since this approximation of muscle force neglects about 10% of force contribution from muscles with smaller moment arms, we expect our overall

estimate of muscle force and tibia force to be lower than the actual forces, but within a reasonable range of error.

Section 1.2.2 Accuracy of Lab-Based Tibia Force Estimates

Utilizing the inverse dynamics approach outlined above, we are able to estimate bone loading using data easily obtained in a motion capture lab with a force instrumented treadmill. More complex musculoskeletal models have been developed to estimate forces in the lower limbs during locomotion (Arnold, Ward, Lieber, & Delp, 2010; Erdemir, McLean, Herzog, & van den Bogert, 2007; Horsman, Koopman, Helm, Prosé, & Veeger, 2007), but recent research has shown that differences between estimates using the simplified inverse dynamics method and the more complex musculoskeletal modeling methods are minimal, suggesting that the inverse dynamics approach is sufficient for this application (Kernozek, Gheidi, & Ragan, 2017). Kernozek's study found that peak Achilles tendon force (a main contribution in tibia force) estimated using inverse dynamics and static optimization through modeling differed by less than five percent.

In order to compare estimates of total tibia loading to a real "ground truth" in a living subject, instrumented tibial prostheses equipped with telemetry devices (D'Lima, Patil, Steklov, Slamin, & Colwell, 2006; Kaufman, Kovacevic, Irby, & Colwell, 1996) can be used to measure tibia forces during walking experiments. Peak tibia forces measured by these devices are lower than the average values estimated via the inverse dynamics approach, but are within a similar range of two to three body weights for walking (D'Lima et al., 2006; Mündermann, Dyrby, D'Lima, Colwell, & Andriacchi, 2008; Taylor, Walker, Perry, Cannon, & Woledge, 1998). D'Lima reported the results from an instrumented knee for a single subject recovering from a

total knee arthroplasty and found a peak tibia force of 2.17 body weights during walking at six weeks post-operation. Similarly, Mündermann found that 18 months post-operation, one subject with an instrumented knee prosthesis experienced peak tibia forces of about 2.5 body weights during walking. Taylor tested one subject with an instrumented prosthesis during walking at one year post-operation and found peak loads of 2.51 body weights at the fastest walking speed. All three studies report lower peak tibia forces than the averages from studies using lab-based estimates (Morrison, 1970; Thambyah, Pereira, & Wyss, 2005), but loading cycles follow the same trajectory across all studies. It is also worth noting that all peak loads fell within the range of values reported by Morrison. The lower values in the single subject experiments could easily be attributed to different walking speeds or the fact that subjects with instrumented knee prostheses were much older than subjects in Morrison's and Thambyah's experiments.

Section 1.3 Wearable Technology for Health Monitoring

With the rise of technology in everyday life, the variety and quality of sensors used for measuring biomechanical data has seen a substantial increase, and many of the technologies used in current products may be useful in a device to measure bone loading. Fitness trackers, such as smartwatches and smartphone apps (i.e. Fitbit, Garmin) have become increasingly popular, and help people monitor their own health and fitness. Some products have features that help users lose weight and eat healthier, and others simply keep track of data such as number of steps or flights of stairs climbed each day. With more and more sensors available, it is becoming increasingly practical to output more actionable measures which can improve users' health by helping to predict and reduce injury. Since sensors are now becoming smaller, cheaper, and more widely available, the feasibility of making a portable device to measure and analyze gait for the

purposes of injury prevention while remaining comfortable and affordable is increasing. However, before a device or product is created, we must first determine the types of sensors we wish to use, and in which locations on the body. There are already a variety of sensors available to measure biomechanical data; the goal of this study is to collect data from a target subset of sensors and determine whether it is feasible to estimate tibia bone forces with data from these sensors.

Section 1.3.1 Existing Wearable Sensors

A variety of sensors are available and currently used in laboratory settings to measure biomechanical data beyond permanent measurement systems such as force plates, treadmills, and motion capture cameras. It is our hope that these sensors will be able to provide sufficient data to estimate tibia bone loading, and that these sensors can be integrated into a wearable device that will enable data collection outside of the lab. Below is a summary of the current capabilities of the types of wearable sensors used in this experiment.

Section 1.3.1.1 Pressure Insoles

A variety of pressure sensing insoles are available to be placed inside a subject's shoe and measure the forces applied throughout the gait cycle. Most of these insoles are composed of a series of individual sensors places across the foot, but the size and number of these sensors varies greatly between products. Typically, insoles record a single vertical force measurement of the force normal to the insole, while instrumented treadmills and force plates record three-dimensional ground reaction forces. Some insoles are also able to provide an output of center of

pressure. Pressure insoles are likely to be useful for ground reaction force estimates, although the forces and center of pressure output by the insoles are with respect to the shoe as opposed to the ground, so resolving into a global coordinate frame may be necessary for accurate calculations.

Section 1.3.1.2 Accelerometers

In order to obtain information about the velocity, acceleration, and orientation of different segments of the body, accelerometers are often used. These sensors often include gyroscopes and magnetometers, resulting in a wider range of output variables. Sophisticated accelerometers can be calibrated and perform filtering in order to obtain accurate representations of rotation/orientation. A combination of accelerometers may be used to determine segment and joint angles as well as the velocities or accelerations of segments of the body, particularly the foot and lower leg.

Section 1.3.1.3 Electromyography Sensors

Electromyography sensors are often used in conjunction with laboratory measurements to verify muscle activity by measuring electrical signals across the muscle. These sensors may be wired or wireless and come in different sizes and with different capabilities. With data processing, electromyography measurements can be used to compare relative activation of a muscle across different portions of the gait cycle, which may be useful in comparing the relative forces produced by the calf muscles during running. While not directly related to the initial derivation of tibia force proposed in this study, electromyography sensors may be useful in later

iterations of data processing that incorporate machine learning or other data compilation algorithms.

Section 1.3.2 Existing Running Trackers

Many products claiming to provide feedback on running mechanics and injury risks are beginning to appear on the market and represent both progress and interest in more sophisticated wearable technology. Most of these products are confined to an insole or attachment to the shoe, measuring forces or accelerations of the feet to calculate output metrics from stride data to running pace to power and technique analysis. Several of these portable products, such as IMeasureU, output shock as a metric which may be correlated to stress fracture injury, however there remains little evidence to support this claim. Other companies, such as Ziel and Motus have developed arm sleeves for athletes such as baseball pitchers or football quarterbacks to prevent upper extremity injuries. Another common type of product is a wearable sensor that attaches to the body through straps or pockets, and often records accelerometer data to determine output metrics (i.e., Xsens). In general, the wearable technology available to the public advertises improving force balance, efficiency, or loading pattern during running, which they claim to be indicative of a lower risk of stress fractures. However, depending on the person, the most balanced or efficient running style may not be the best for minimizing injury, since injury risks are more complicated than simple energy consumption variables (Bennell et al., 1999). While these devices aim to evaluate injury risks, all products currently on the market use an indirect approach to determine potential risk factors. The approach proposed in this study is unique because we seek to calculate a direct estimate of tibia bone loading, the underlying cause of bone

stress fracture, rather than external metrics (e.g., ground reaction force or foot acceleration) which may or not correlate with bone loading or injury risk.

Section 1.3.3 Motivation for Portable Bone Load Estimation

In order to analyze recreational runners and assess their risk of developing a stress fracture in their natural training environments and over longer periods of time than in a laboratory setting, it is necessary to develop a wearable device that can accurately and reliably measure tibia bone loading. While we can confidently estimate tibia bone loading on a treadmill or force plate in the laboratory, the number of conditions that can be tested are limited. For example, rugged terrains, turns, and continuously varying slopes cannot be easily recreated in a laboratory setting, yet are common in daily running routines of most athletes. Capturing within-run and between-run variability is useful for understanding changes in bone loading and the onset and development of pain and injury. Additionally, there is reason to believe that changes in bone loading patterns that cause stress fractures may not be reproducible in a lab setting. For example, if a runner changes their muscle coordination during a long run due to fatigue, this may not be captured in shorter lab trials. Therefore, it would be beneficial to have a strong surrogate for laboratory estimates of bone loading, composed of wearable sensors that can measure at any time and in any location to allow for a wider breadth of data collection that is more representative of everyday running.

Section 1.4 Objectives

Given the prevalence of stress factors, particularly of the tibia, among the population of recreational runners, there is a clear need for a more comprehensive understanding of tibia bone loading and for a method and device used for measuring bone loading across longer periods of time and running conditions than producible in a laboratory setting. As such, the objectives of this experiment are twofold. First, test a set of running conditions that yield different bone loadings and synchronously collect lab data and wearable sensor data for all conditions. Then, with the data obtained, calculate tibia bone loading using lab-based estimation methods and wearable sensor-based estimation methods and determine the range of accuracy of wearable sensor-based estimates calculated using an inverse dynamics approach.

It is presently unknown which features are most interesting or useful for predicting stress fractures, in large part because of the lack of prospective studies and validated sensors that can track bone loading in daily life. Based on prior literature, we have selected a few summary metrics that characterize aspects of bone loading that might provide predictive values. Specifically, we are interested in answering the following question: within what root mean square error can a) tibia bone loading, b) peak tibia load, and c) tibia load per kilometer be estimated during the stance phase of gait using wearable sensors?

Section 1.4.1 Scope and Methodology

Many factors, both intrinsic and extrinsic, influence the load that the tibia experiences during running; the goal of this experiment is to test a variety of conditions yielding different tibia loadings so that the feasibility of estimating tibia bone load using wearable sensors can be

analyzed. For this study, variations in step frequency and speed will be tested as a representative sample of factors that could be varied in an athlete's training regimen. In order to directly compare laboratory-based estimates (lab estimates) of tibia force to wearable sensor-based estimates (wearable estimates), collection of all data will occur simultaneously and synchronously. Motion capture markers will be placed on the subject in addition to all wearable sensors, and trials will be performed on a force instrumented treadmill in order to ensure similar conditions for all subjects and all trials.

Once sufficient data has been collected, the second aim of this study will be to determine the accuracy of wearable estimates of tibia bone loading by investigating the correlations between lab based and wearable estimates of tibia load, peak tibia load, and tibia load per kilometer. Using an inverse dynamics approach, lab data will be used to estimate the tibia bone force profile, peak tibia force, and tibia load per kilometer. Wearable estimates of tibia bone loading will be calculated using the same approach as for the lab estimates of tibia bone loading, modifying the equations by replacing lab data with wearable surrogates: pressure sensing insoles to replace the force instrumented treadmill force and center of pressure measurements, and an inertial measurement unit to replace motion capture-based joint angles.

Section 1.4.2 Hypothesis

Our hypothesis is that wearable estimates of tibia bone load can approximate lab estimates of tibia bone loading within a root mean square error of less than ten percent peak loading for each metric analyzed (tibia force over stance, peak tibia force, and tibia load per kilometer).

Chapter 2: Methods

Section 2.1 Condition Selection

In order to assess the accuracy of wearable estimates of tibia force in different circumstances, tasks were selected to represent a range of bone loading typical in recreational running. Many conditions were tested in the experimental protocol, but for the purposes of this preliminary investigation, only tasks varying step frequency at a constant speed on level ground, and varying speeds on level ground, were analyzed.

Previous studies have found significant differences in various running mechanics metrics, including segment orientations, ground reaction force, acceleration, and leg stiffness, across different running step frequencies (Schubert, Kempf, & Heiderscheit, 2014). Studies have shown that an increase in step frequency results in lower initial impact peaks and loading rates in ground reactions forces (Hobara, Sato, Sakaguchi, Sato, & Nakazawa, 2012), lower peak ground reaction forces (Farley & González, 1996; Heiderscheit, Chumanov, Michalski, Wille, & Ryan, 2011). More generally, increases in step frequency yield lower ground reaction forces throughout stance (Morin, Samozino, Zameziati, & Belli, 2007), as seen in Figure 4.

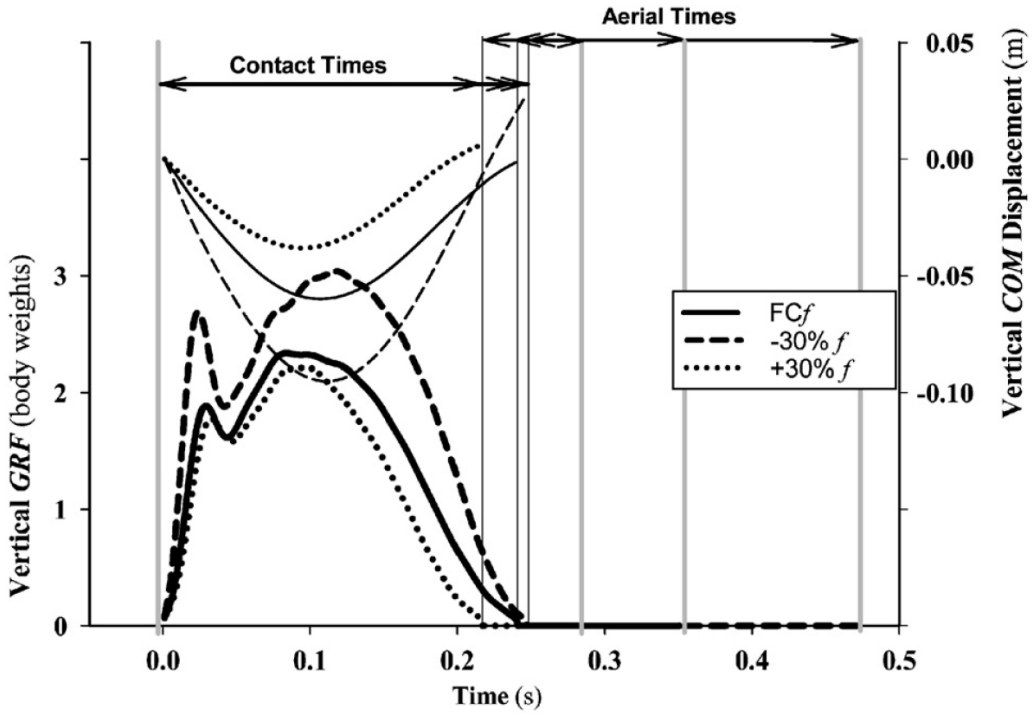

Figure 4. Results from Morin et al. showing a decrease in vertical ground reaction force with an increasing step frequency during running.

While previous studies tested various ranges of step frequencies, most found statistically significant differences in output metrics at 10-20% deviations from preferred step frequency. Pilot testing was conducted to determine the largest deviations from preferred step frequency that could be comfortably performed by subjects while running on the treadmill. Based on this pilot testing and results from previous studies, we decided to test step frequencies between -15% and +15% of preferred step frequency, which we expect to yield a range of tibia bone loading curves suitable for evaluating our wearable estimates.

For this study we will also record running trials at different speeds to assess wearable estimates over a wider range of conditions. Running speed has been shown to alter lower limb bone strain in goats, dogs, and horses, where an increase in speed results in an increase in strain

on the tibia bone, as shown in Figure 5 (Biewener & Taylor, 1986). We expect to see an increase in tibia bone loading with an increase in speed in humans as well. Slow running speeds, between 2.2 and 3.0 m/s were chosen in order to accommodate subjects who were inexperienced runners.

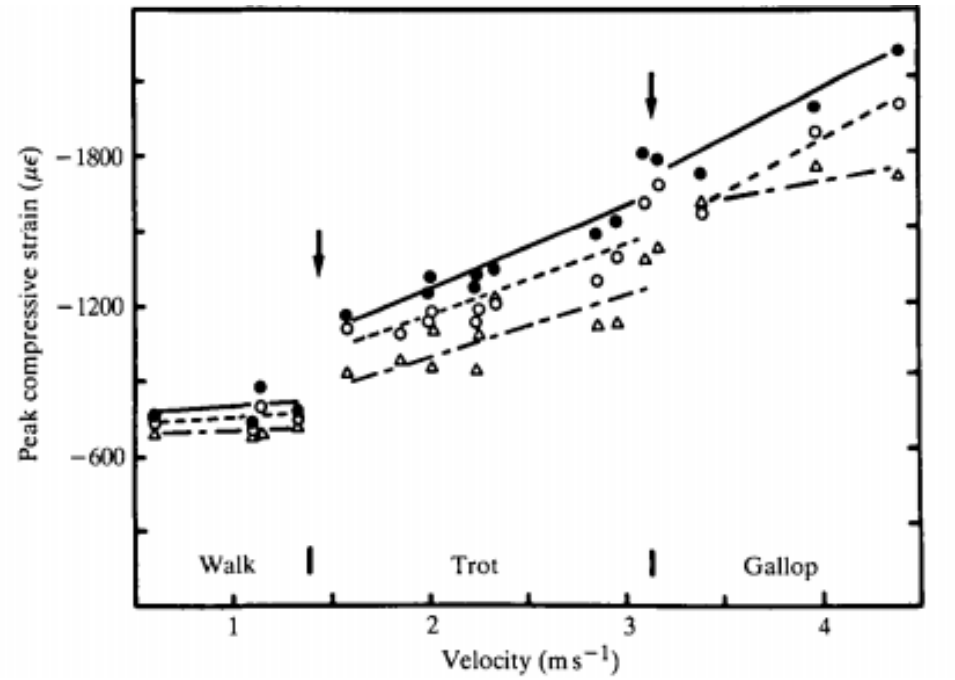

Figure 5. Results from Biewener & Taylor showing an increase in compressive strain on the goat tibia with increasing running velocity.

Section 2.2 Experimental Design

In this experiment, sensor placement and synchronization were extremely important in order to ensure both an accurate lab estimate of tibia loading and a corresponding set of portable sensor data for analysis. Since the goal of this experiment is to determine if wearable sensors are capable of calculating bone loading for most or all subjects, special care was taken to use similar

sensor placement during each data collection. With so many measurement modalities being utilized at once, extra emphasis was also placed on designing a repeatable and robust experiment.

Section 2.2.1 Data Collection Hardware

Prior to subject arrival, data collection software was prepared, sensors were cleaned, charged, and organized, and motion capture hardware was calibrated. All trials were performed on a fully-instrumented, split-belt treadmill (Bertec Corporation, Columbus, OH) capable of measuring forces, moments, and centers of pressures at 1000 Hz on each belt. A ten camera motion capture system (Vicon Motion Systems, UK) was used to record lower limb motion at 200 Hz during all trials.

Section 2.2.2 Subject Preparation

Three healthy adult subjects (2 male, 1 female, height 1.8 ± 0.1 m, weight 66.8 ± 7.0 kg, age 24.6 ± 1.5 years) participated in this study. Inclusion was determined based on physical fitness (ability to complete all trials) and shoe size (within the range of available insole sizes). Upon arrival, subjects were given an overview of the experimental protocol and goals, then gave informed consent to participate in the study (approved by the Vanderbilt University Internal Review Board). Subjects were instructed to wear tight-fitting shorts to facilitate motion capture marker placement. While on the treadmill, subjects wore an upper body safety harness which was secured via a belay system to the ceiling. Handrails were attached to the treadmill on either side of the subject and an emergency stop button was affixed to the railing for subject safety.

Given the high number of measurement modalities used on the lower limbs, care was taken to avoid overlapping or obstructing sensors. With this goal in mind, pressure sensing insoles were set up first, followed by the inertial measurement unit, and finally motion capture markers. A schematic of the experimental setup is shown in Figure 6 and labeled images of all sensors on a subject can be found in the Appendix.

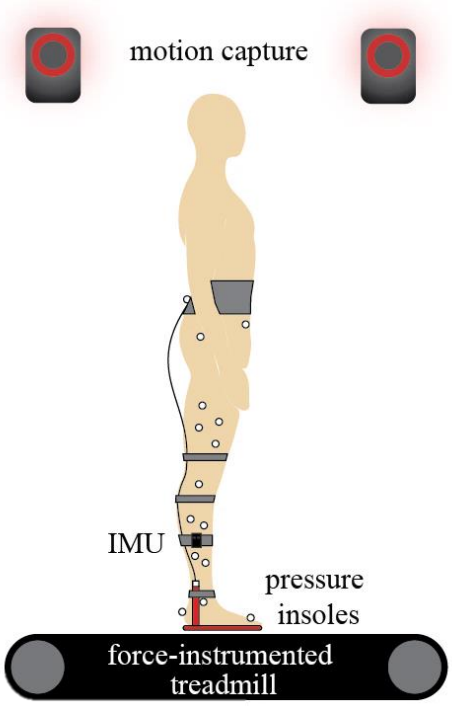

Figure 6. Experimental setup schematic, with motion capture cameras and markers on the lower limbs, a force instrumented treadmill, pressure-sensing insoles in the shoes with associated data collection hardware/electronics on the abdomen, and an inertial measurement unit on the shank.

The Pedar-X pressure sensing insole system (Novel, Munich, Germany) was set up for collecting data under each foot. A belt carrying the portable electronics (main collection box, battery, synchronization unit) was strapped to the subject's abdomen and insoles were placed inside each of the subject's shoes. Insoles were connected via cables to the main collection box

and straps were placed at the ankle, calf, and thigh to secure the cables to the subject's legs. Insoles were tared and then subjects tied the laces of their shoes as desired.

With the pressure sensing insoles set up, the 3-Space Data Logger inertial measurement unit (Yost Labs, Portsmouth, Ohio) was placed on the right shank. The IMU was placed on the lateral part of the shank using Velcro and a fabric strap such that the IMU's y-axis was parallel to the knee axis and its z-axis was aligned with the shank. After placement, the sensor was tared while the subject stood in an upright, natural position.

Once all wearable sensors were in place, twenty-four reflective motion capture markers were placed on landmarks and segments of the subject's pelvis and right leg to record lower limb kinematics: six on the pelvis, four in a cluster on the thigh, two on the knee, four in a cluster on the shank, two on the ankle, and six on the foot. Markers were attached to the body using double sided tape, and additional tape was placed around the markers on the shoes and any particularly sweaty areas to prevent markers from moving or falling off during data collection.

Section 2.2.3 Data Collection

Data collection for this study consisted of four sets of conditions: calibration trials, decreasing step frequency trials, increasing step frequency trials, and speed sweep trials. All trials were performed on the treadmill at zero incline. The experiment began with one static and two functional calibrations, used to define motion capture marker placements and joint locations as well as obtain baseline force and orientation measurements. After this, the treadmill was turned on and set to a moderate walking speed to allow subjects to acclimate to the treadmill. Once comfortable, the treadmill was then set to a moderate running speed (2.4 m/s or 2.6 m/s),

and subjects ran at their preferred step frequency. Once at steady state, experimenters counted the number of strides taken during a thirty second period and doubled this number to obtain subjects' preferred step frequency. Once this measurement was completed, the treadmill was stopped and subjects were allowed to rest.

Two running step frequency condition sweeps were performed, each comprised of four trials, beginning with the subject running at their natural step frequency, then increasing or decreasing the step frequency by five percent per trial. All trials were performed at a constant running speed of 2.4 m/s or 2.6 m/s, corresponding to the speed of the calibration trial. For each trial, a metronome was set and played over speakers to regulate step frequency, with one beat played for each desired foot strike. Subjects began standing on the treadmill at the beginning of each trial, stomped on the treadmill with the right foot, and were then brought to their running speed and instructed to match their foot strikes to the beat of the treadmill. Once synchronized with the metronome, twenty to thirty additional seconds were recorded before stopping the treadmill and resetting for the next trial.

Upon completion of the step frequency trials, speed sweep trials were conducted. Four trials were recorded for each subject, beginning at 2.2 m/s or 2.4 m/s and increasing by 0.2 m/s for each trial. All trials occurred with the treadmill set to zero incline, and no metronome was playing during speed sweep trials so subjects were free to self-select their step frequency for each trial. Trials were conducted one at a time in a similar fashion to the step frequency sweep: subjects began standing still on the treadmill, stomped before the treadmill was set to the desired speed, and once at the steady state speed, ran for twenty to thirty seconds in order to collect sufficient data to analyze before the treadmill was stopped and reset for the next trial.

In order to synchronize the various measurement modalities, several methods were employed. Motion capture, treadmill force, moment, and center of pressure data were collected using Vicon's Nexus software. Insole pressures were collected separately at 100 Hz through Novel's Database and Pedar data collection software. Using Novel's synchronization system, an analog signal was recorded in Nexus and used to trigger the start of data collection for each trial whenever the experimenter began a trial in the Pedar software. Trials were stopped manually in Nexus and Pedar upon completion of the twenty to thirty second steady state segment of running but prior to stopping the treadmill. Euler angles calculated by the IMU utilizing a Kalman filter were collected separately at approximately 60 Hz and stored locally to the IMU device. Experimenters pressed the record button on the IMU at the beginning of each trial and the stop button upon completion of each trial once the treadmill reached a stop. This data was synchronized and trimmed to match other data by aligning the peaks corresponding to the stomp at the beginning of each trial. For analysis purposes, twenty second segments at the end of each trial were isolated for analysis.

Section 2.3 Data Processing

Using the static calibration trial for each subject as a model, motion capture marker labeling and gap filling was performed in Vicon's Nexus software, and exported into Visual3D (C-Motion, Germantown, MD) for model-based calculations and data exporting. The functional calibration trial was used to define functional joints which enabled the calculation of joint-based kinematic and kinetic metrics. Motion capture data was filtered using a fourth order Butterworth filter with a cutoff frequency of 6 Hz and treadmill data was filtered with a cutoff frequency of 15 Hz. Complete ground reaction forces, shank angles, and ankle moments were exported into

Matlab for further calculations. Pedar data files containing force and center of pressure measurements, and Yost data files containing Euler angles were imported and saved in a Matlab data file in a structure containing all other data from the study. Using a custom Matlab script, data was aligned using the peak in force from the stomp at the beginning of each trial, and all sources of data were trimmed to twenty seconds. Once trimmed, data was parsed to identify heel strike and toe off events, separate data intro strides, and average over the number of strides in the twenty seconds of data. The result of this processing is single vector of one thousand data points for each metric corresponding to the stance phase of one gait cycle.

Section 2.4 Data Analysis

As described in Introduction, tibia force can be approximated as the sum of external and internal forces. Estimation methods for each force differed between lab and wearable techniques, but the same general principle of summing forces, as described in Equation 1, applies for each. All calculations described below were done using a custom Matlab script, and data for each trial was saved into subject-specific structures.

$$F_{tib} = \Sigma F = F_{ext} + F_{int} \quad (1)$$

Section 2.4.1 Laboratory Estimates of Tibia Force

Using Equations 2 and 3, and the outputs from Visual3D, lab-based external (ground reaction force) and internal (muscle) contributions to tibia force were estimated. External force was estimated as the ground reaction force vector projected onto the long axis of the tibia (Equation 2). The tibia axis was estimated as a vector from the computed ankle joint center to the

knee joint center. Internal force was estimated as the ankle moment divided by the moment arm of the Achilles tendon, assumed to be a constant value of 5 cm (Equation 3). Because the force contributions of dorsiflexor muscles was ignored, any period of negative ankle moment following heel strike was set to zero.

$$F_{ext,lab} = \left|\overrightarrow{GRF}\right| * \cos\theta_{tib-GRF} \quad (2)$$

$$F_{int,lab} = \frac{M_{ankle}}{|r_{AT}|} = \frac{\overrightarrow{r_{COP-ankle}} \times \overrightarrow{GRF}}{|r_{AT}|} \quad (3)$$

Section 2.4.2 Wearable Estimates of Tibia Force

Using Equations 4 and 5 (modifications of Equations 2 and 3) and the data from the pressure sensing insoles and inertial measurement unit, wearable sensor-based external (ground reaction force) and internal (muscle) contributions to tibia force were estimated. External force was estimated as the vertical ground reaction force as measured by the insoles projected onto the axis of the tibia in the sagittal plane, using the shank angle from the IMU (Equation 4). Internal force was estimated as the product of insole-based center of pressure to ankle moment arm (measured center of pressure minus an assumed constant distance from the heel to the tibia/ankle of 5 cm) divided by the moment arm of the Achilles tendon, assumed to be a constant value of 5 cm (Equation 5).

$$F_{ext,wear} = GRF_{vertical} * \cos\theta_{shank} \quad (4)$$

$$F_{int,wear} = \frac{(|\overrightarrow{r_{COP,insole}}| - |r_{heel-tib}|) * GRF_{vertical}}{|r_{AT}|} \quad (5)$$

Section 2.4.3 Peak Tibia Force and Tibia Load per Kilometer

Once waveforms of tibia force were generated for each trial, two other metrics were calculated. First, peak tibia force was determined, as described in Equation 6, as the maximum value of tibia force for each trial. Peak force was determined for both lab and wearable data sets.

$$F_{tib,peak} = \max(F_{tib}) \tag{6}$$

Tibia load per kilometer was calculated as a metric that may give insight into loading of the tibia over time. Tibia load per kilometer was calculated as tibia load per step multiplied by the rate of steps per kilometer for each trial (Equation 7). Tibia load per step is defined as the impulse, or area under the tibia force-time curve during stance, and rate of steps per kilometer for each trial was defined as the reciprocal of the product of stride time and treadmill velocity. Load per kilometer was determined using lab and wearable tibia force data, but stride time and velocity were determined from the treadmill for all cases. Stance time was the time from heel strike on one food to toe off on the same foot. Stride time was the time from heel strike on one foot to the following heel strike on the same foot.

$$J_{tib\ per\ km} = J_{tib\ per\ step} * \frac{steps}{km} = \frac{\int_0^{t_{stance}} (F_{tib} * dt)}{t_{stride} * v_{treadmill}} \tag{7}$$

Section 2.4.4 Calibration of Wearable Estimates

Due to inherent error in wearable sensor data and the use of modified equations, we do not expect perfect estimates of tibia load. In order to correct for these inaccuracies, we will determine the linear trendline that minimizes error between lab and wearable estimates of tibia force over stance. This trendline will account for a scaling factor and constant offset between lab

and wearable estimates. Using the trendline equation, wearable sensor data will be recalculated as the raw estimate times the scaling factor and plus the constant offset. This new, calibrated wearable estimate of bone loading will be used to compute error between lab and wearable estimates. Rather than focusing on the absolute value of tibia force estimates, this approach will allow us to evaluate whether trends in lab estimates of tibia bone load are also estimated in wearable estimates. Calibrations will be determined for individual trials, single subjects, and all subjects.

Section 2.4.5 Calculation of Error

For all metrics, root mean square error (RMSE) was found between lab and raw wearable estimates, as well as between lab and calibrated wearable estimates. RMSE is reported in body weights for force over stance and peak force, and in body weights times seconds for load per kilometer. RMSE is also given as a percentage of maximum for each metric, where the maximum is defined to be the maximum force (for force over stance and peak force) or load per kilometer recorded within the set of data analyzed (i.e., a single condition for trial by trial analysis, all conditions for a single trial for subject by subject analysis, or all trials for overall analysis).

Chapter 3: Results

Section 3.1 Laboratory Estimates of Tibia Force

Utilizing lab measurements, tibia loads were estimated using the inverse dynamics approach explain in Methods, and analysis of differences between conditions was performed. As discussed in the Introduction, external (i.e. projected ground reaction) and internal (i.e. muscles and tendons) forces contribute to total tibia force. In this study, it was found that external forces produce a force on the tibia equivalent to 1.5 to 2.4 body weights, whereas internal forces produce a force on the tibia of 3.2 to 6.2 body weights, resulting in a total tibia loading of 4.4 to 8.1 body weights in the conditions tested. An example plot from a representative trial is shown in Figure 7, where it can be seen that during early stance, external forces comprise most of the total tibia force, but in mid to late stance, the contributions of internal forces are up to 3.8 times the contributions of external forces.

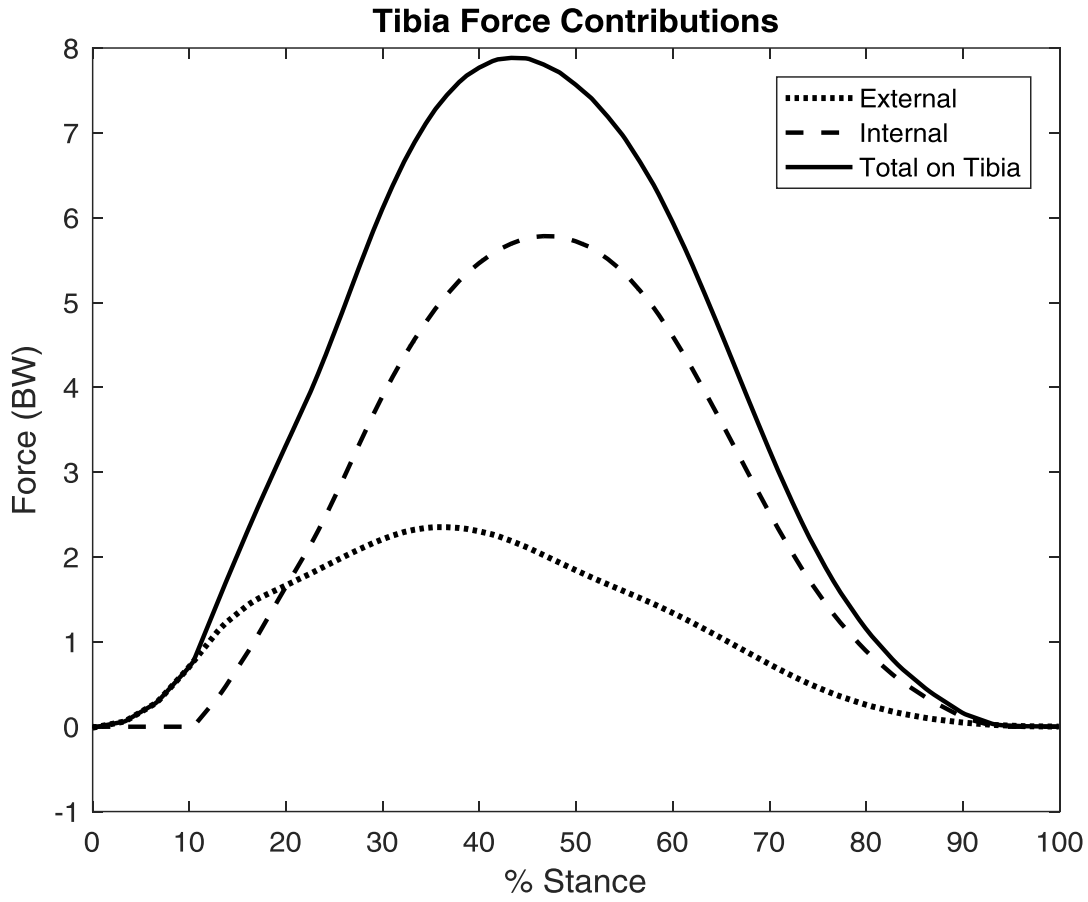

Figure 7. Experimental results showing contributions of external and internal force components to total tibia force. Data shown is from a representative trial.

Section 3.2 Condition Comparisons

Between conditions, differences in magnitudes and timing of tibia loading were observed. Summaries of differences in step frequency, stance times, and peak tibia loads calculated from lab measurements are included in Tables 1-3. In the tables, step frequency sweep trials (SF) are labeled by percent deviation from preferred step frequency and were all completed at 2.4 m/s for subject 1 and 2.6 m/s for subjects 2 and 3, while speed sweep trials (SP) are labeled by treadmill speed in meters per second. Step frequencies are given in steps per minute, stance time is given

in seconds, and peak tibia load is given in body weights. In all but one case, increasing step frequency resulted in a decreased stance time for all subjects. A plot of peak tibia loads (in body weights) versus step frequency (in percent deviation from preferred step frequency) and speed (in m/s) is shown in Figure 8, where each subject is denoted by a different color marker on the plot. In general, peak tibia forces increased with positive deviations from preferred step frequency, while differences in peak tibia forces for negative deviations from preferred step frequency varied between subjects. For the speed sweeps, step frequencies and peak tibia forces tended to increase with increasing speed, while stance time tended to decrease with increasing speed.

Table 1. Summary of differences in in step frequency, stance time, strides per kilometer, and peak tibia force across all trials performed by Subject 1.

	SF -15	**SF -10**	**SF -5**	**SF +0**	**SF +5**	**SF +10**	**SF +15**	**SP 2.2**	**SP 2.4**	**SP 2.6**	**SP 2.8**
Prescribed Step Freq.	72	76	80	84	88	92	96				
Actual Step Freq.	72.8	75.9	80.4	84.3	88.8	92.6	96.6	78.1	81.7	84.2	83.9
Stance Time	0.39	0.40	0.36	0.36	0.35	0.35	0.33	0.40	0.37	0.35	0.34
Strides Per Kilometer	505	527	559	585	616	643	670	592	567	540	500
Peak Tibia Force (Lab)	5.99	5.82	5.91	5.44	5.22	4.78	4.35	5.26	5.38	5.53	5.56

Table 2. Summary of differences in in step frequency, stance time, strides per kilometer, and peak tibia force across all trials performed by Subject 2.

	SF -15	SF -10	SF -5	SF +0	SF +5	SF +10	SF +15	SP 2.4	SP 2.6	SP 2.8	SP 3.0
Prescribed Step Freq.	72	76	80	84	88	92	96				
Actual Step Freq.	72.6	75.5	80.3	83.9	88.1	92.3	96.3	83.0	83.0	83.8	86.2
Stance Time	0.35	0.34	0.32	0.30	0.28	0.26	0.25	0.30	0.30	0.30	0.29
Strides Per Kilometer	466	484	515	538	565	592	617	576	532	499	479
Peak Tibia Force (Lab)	7.40	7.59	7.57	7.57	7.47	7.26	7.07	7.35	7.73	7.88	8.06

Table 3. Summary of differences in in step frequency, stance time, strides per kilometer, and peak tibia force across all trials performed by Subject 3.

	SF -15	SF -10	SF -5	SF +0	SF +5	SF +10	SF +15	SP 2.4	SP 2.6	SP 2.8	SP 3.0
Prescribed Step Freq.	72	76	80	84	88	92	96				
Actual Step Freq.	71.8	75.5	80.1	84.1	88.4	92.8	97.0	81.5	82.4	83.5	83.8
Stance Time	0.34	0.34	0.32	0.30	0.28	0.26	0.25	0.31	0.31	0.30	0.30
Strides Per Kilometer	460	484	514	539	567	595	566	528	497	465	465
Peak Tibia Force (Lab)	7.59	7.74	7.79	7.88	7.23	7.00	7.06	7.32	7.67	7.66	7.68

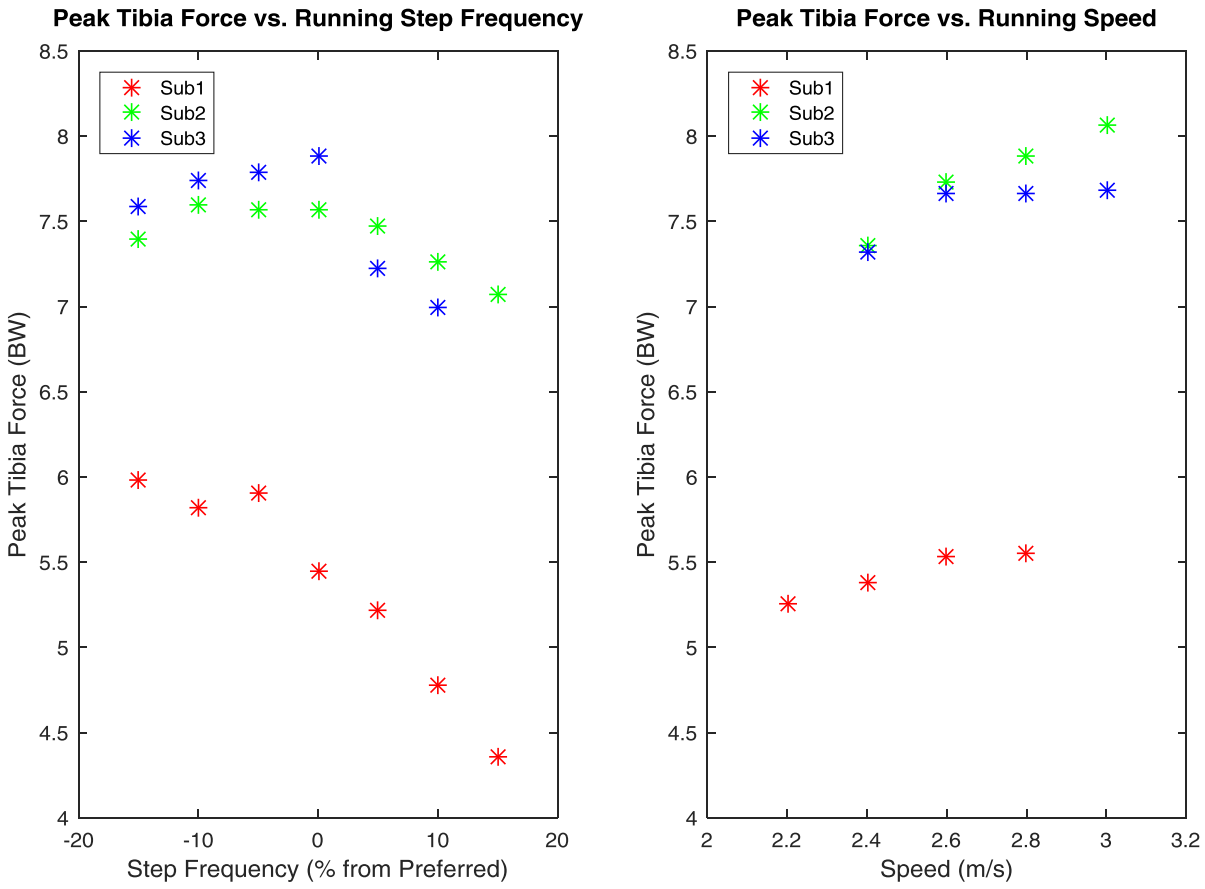

Figure 8. Differences in peak tibia forces for step frequency and speed sweeps of all subjects.

Section 3.3 Wearable Estimates of Tibia Force

Upon completion of lab-based calculations, wearable sensor data was analyzed to assess accuracy of individual measurements as well as overall estimates of tibia forces. In general, the shank angle estimated obtained from the Euler angles of the IMUs were within the correct range of values but did not follow the same curve as the shank angle obtained from motion capture data. Ground reaction force moment arm obtained from insole center of pressure measurements and used to calculate internal contributions to tibia force tended to match measurements from the force instrumented treadmill during early and mid-stance but were overestimated in late stance.

Ground reaction forces measured by the insoles tended to follow the same trajectory as measured ground reaction forces from the treadmill but were slightly delayed in timing during stance and were generally underestimated throughout the stance phase of gait.

Section 3.3.1 Raw Estimates

Wearable sensor data was used in place of lab data to estimate internal and external contributions to tibia force, and to estimate total tibia force experienced during stance. A representative plot of the differences between lab estimates and wearable estimates can be seen in Figure 9. The upper portion of Figure 9 shows the internal, external, and total tibia forces estimated from lab-based measurements in black, and from wearable measurements in pink. In most cases, the wearable estimate displays an underestimate of external forces during early stance and an overestimate of internal and external forces during late stance. During early and mid-stance, the magnitude of total tibia force is lower for the wearable estimate, due to an underestimate of both internal and external forces. The lower portion of Figure 9 shows the error in the total tibia force estimate across the stance phase of gait. For most trials, the magnitude of error between total wearable and lab estimates of tibia force was less than one body weight throughout stance.

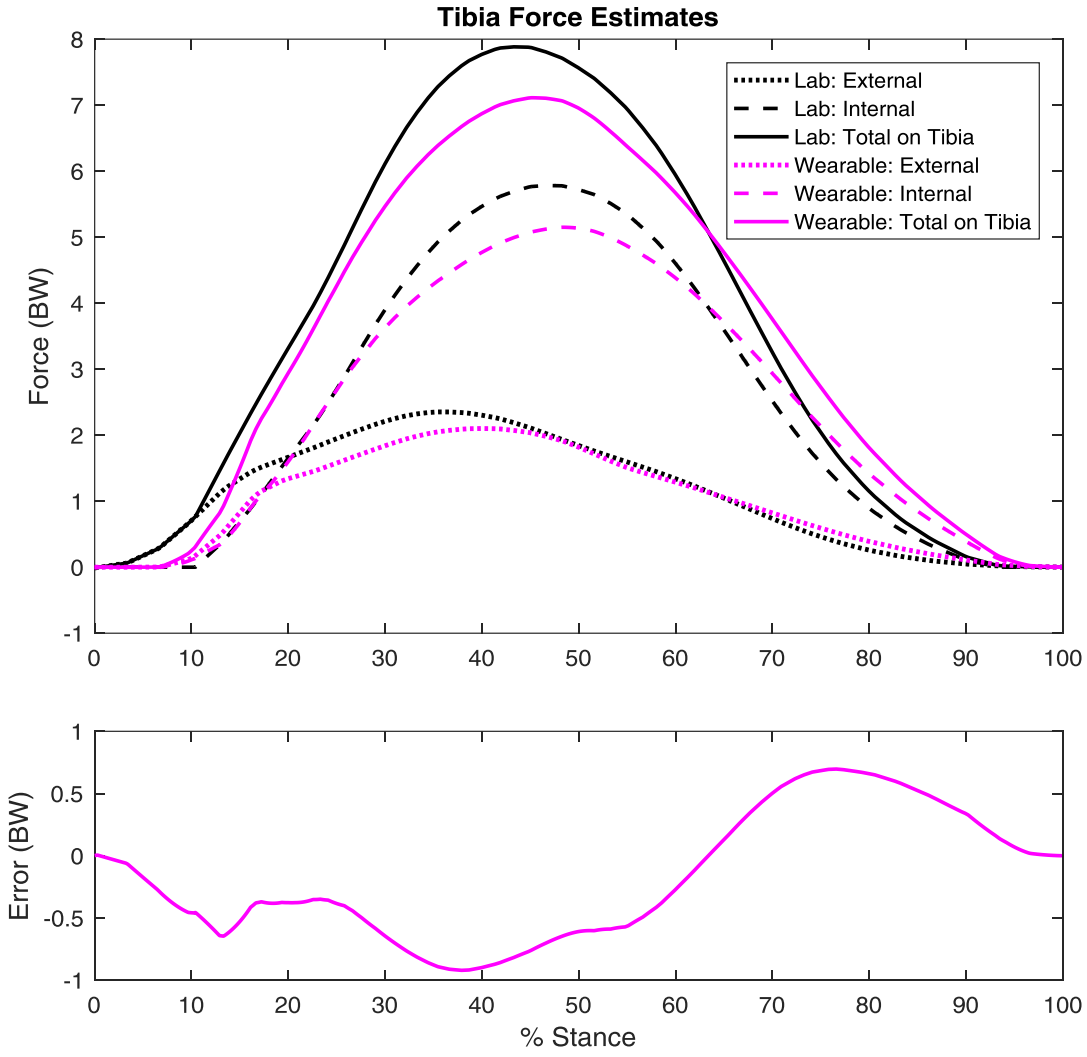

Figure 9. Comparison of lab and wearable estimates of tibia force. Top: differences in estimates of internal, external, and total tibia forces. Bottom: Error between lab and wearable estimates of total tibia force.

As a preliminary analysis to determine the accuracy of the raw wearable estimate of tibia force, the root mean square error between lab and wearable estimates of bone loading throughout the stance phase was calculated for each subject and for all data combined. Subject 1 a root mean square error of 0.70 body weights (11.7% of max). Subject 2 had a root mean square error of

0.82 body weights (10.2% of max). Subject 3 had the lowest root mean square error of 0.46 body weights (5.8% of max). The root mean square error for all subjects was 0.68 body weights (8.4% of max).

Section 3.3.2 Calibrated Estimates

To compare the estimates of total tibia force during stance generated from lab data and wearable data, plots of wearable estimates versus lab estimates were generated for all trials. A linear trendline was fitted to the data for each trial, as well as for all data for each subject, and all data from the study. An example plot is shown below in Figure 10, where the solid line is the data for one representative trial and the dash-dotted line is the best fit line for that single trial. The wearable versus lab estimate curve starts at zero and progresses clockwise on the plot. The best fit line accounts for an arbitrary offset and scaling factor between the two sets of data, and this type of correction could easily be implemented into the processing of data in a wearable device. A plot showing the resulting tibia force curve compared to the raw wearable estimate and the lab estimate of tibia force for a representative trial can be found in Figure 11.

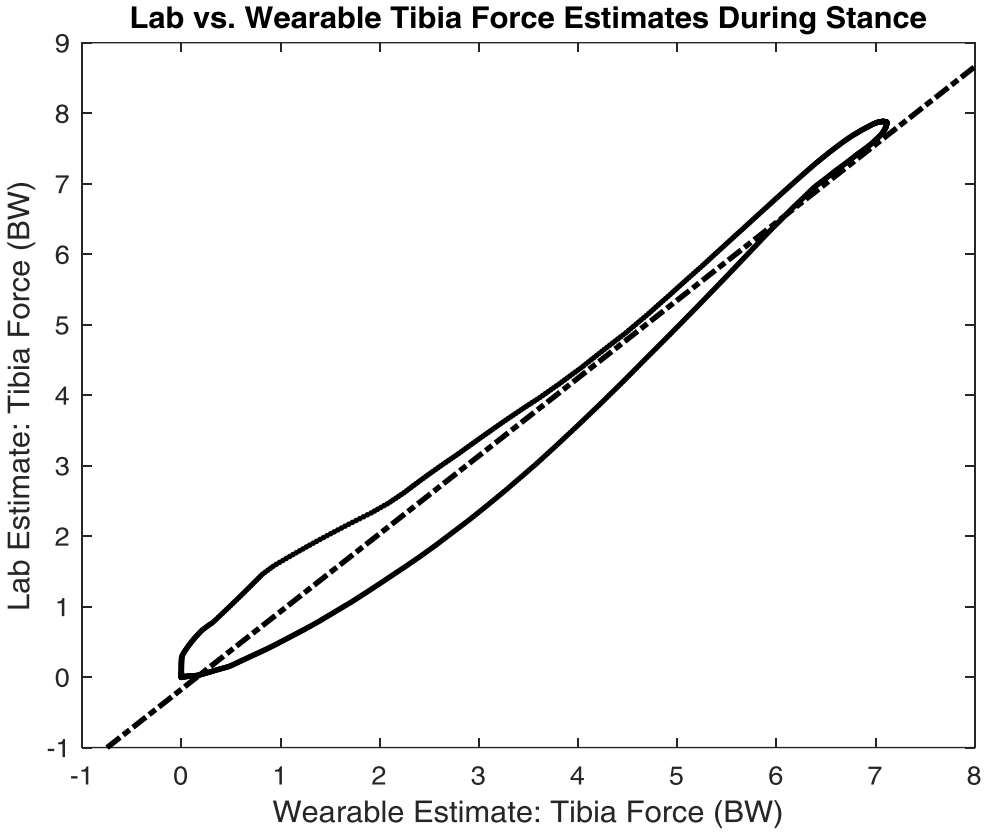

Figure 10. Sample plot of lab estimate of tibia force versus wearable estimate of tibia force during stance with a linear trendline fitted to the data.

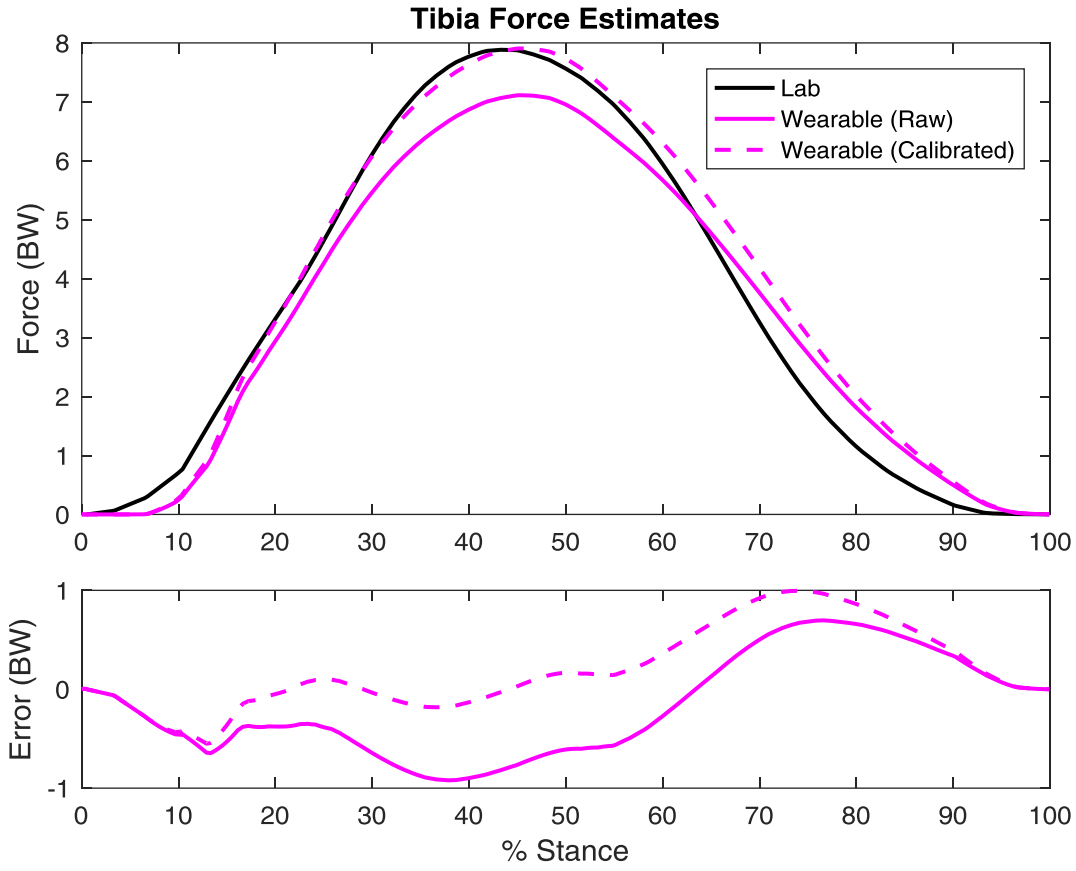

Figure 11. Comparison of lab, raw wearable, and calibrated wearable estimates of tibia force. Top: differences in estimates of total tibia forces. Bottom: Error between lab and raw wearable (solid) and lab and calibrated wearable (dashed) estimates of total tibia force.

From each best fit line, root mean square error of the calibrated estimates was determined for all individual trials, all trials for each subject, and the entire data set. Summaries of these values are included in Tables 4-6. For all trials, root mean square error was less than one body weight, in most cases, well below half a body weight. Subject 1 had the best fit lines with errors less than one quarter body weight (2 to 5% of max). Subject 2 had the greatest errors of between 0.38 to 0.83 body weights (5 to 11% of max). Subject 3 had errors between 0.25 to 0.41 body weights (3 to 6% of max).

Table 4. Root mean square error in trial-specific linear trendline for wearable estimates of tibia force across the entire stance phase of gait for each trial performed by Subject 1.

	SF -15	**SF -10**	**SF -5**	**SF +0**	**SF +5**	**SF +10**	**SF +15**	**SP 2.4**	**SP 2.6**	**SP 2.8**	**SP 3.0**
RMSE (BW)	0.17	0.15	0.12	0.12	0.14	0.20	0.14	0.11	0.12	0.16	0.25
RMSE (% Max)	2.84	2.52	2.03	2.12	2.62	4.14	3.31	2.16	2.27	2.96	4.43

Table 5. Root mean square error in trial-specific linear trendline for wearable estimates of tibia force across the entire stance phase of gait for each trial performed by Subject 2.

	SF -15	**SF -10**	**SF -5**	**SF +0**	**SF +5**	**SF +10**	**SF +15**	**SP 2.4**	**SP 2.6**	**SP 2.8**	**SP 3.0**
RMSE (BW)	0.38	0.46	0.52	0.83	0.61	0.75	0.71	0.47	0.46	0.48	0.48
RMSE (% Max)	5.15	6.06	6.81	10.90	8.14	10.33	10.07	6.43	5.94	6.08	5.90

Table 6. Root mean square error in trial-specific linear trendline for wearable estimates of tibia force across the entire stance phase of gait for each trial performed by Subject 3.

	SF -15	**SF -10**	**SF -5**	**SF +0**	**SF +5**	**SF +10**	**SF +15**	**SP 2.4**	**SP 2.6**	**SP 2.8**	**SP 3.0**
RMSE (BW)	0.39	0.32	0.39	0.41	0.26	0.37		0.34	0.25	0.38	0.27
RMSE (% Max)	5.18	4.10	5.02	5.23	3.55	5.23		4.75	3.36	4.89	3.51

Since the ultimate goal of this work is to develop a wearable sensor that can estimate tibia bone loading during everyday activities, it is important to assess the accuracy of wearable estimates across trials and across subjects rather than for a single trial. Plots containing lab versus wearable estimates of tibia load for all trials for each subject were generated and a line of best fit for the entire data set for a subject was obtained in a similar was as was done for each

trial. These plots are shown below in Figures 12-14 for subjects 1-3 respectively. Results of calibrations for individual subjects are shown in Table 7.

Table 7. Root mean square error in calibrated wearable estimates of tibia force across the entire stance phase of gait for each subject.

	Subject 1	**Subject 2**	**Subject 3**
RMSE (BW)	0.18	0.62	0.34
RMSE (% Max)	3.0%	7.7%	6.1%

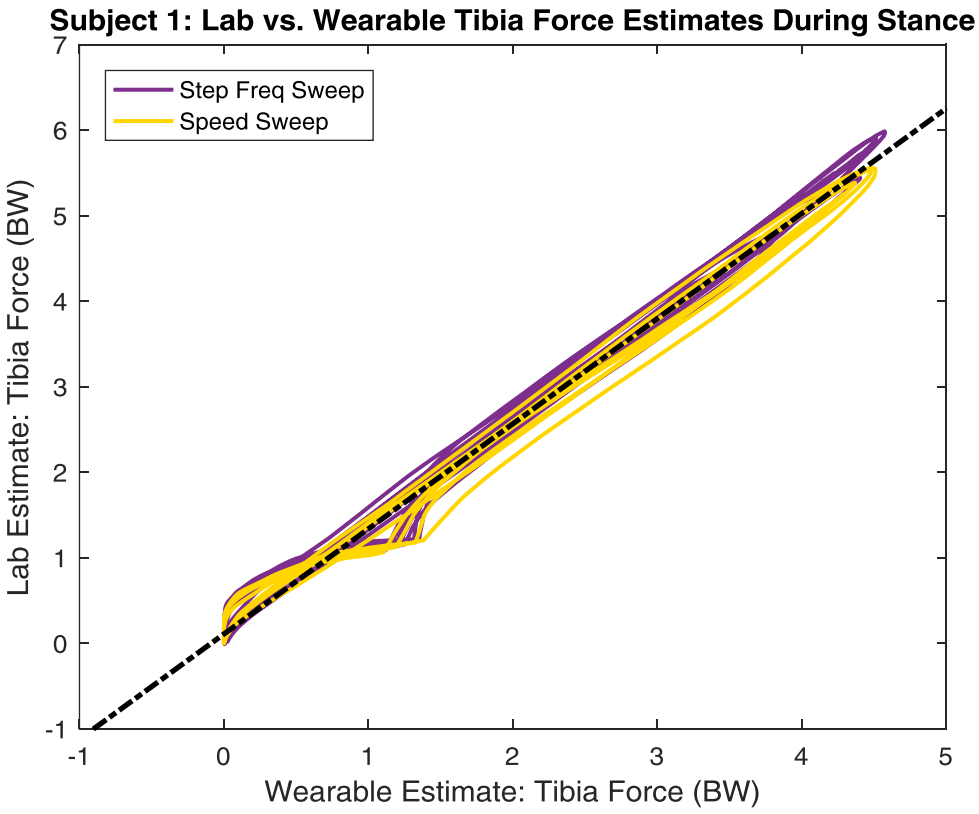

Figure 12. Lab estimates of tibia force versus wearable estimates of tibia force during stance for all trials completed by Subject 1 with a linear trendline fitted to the data.

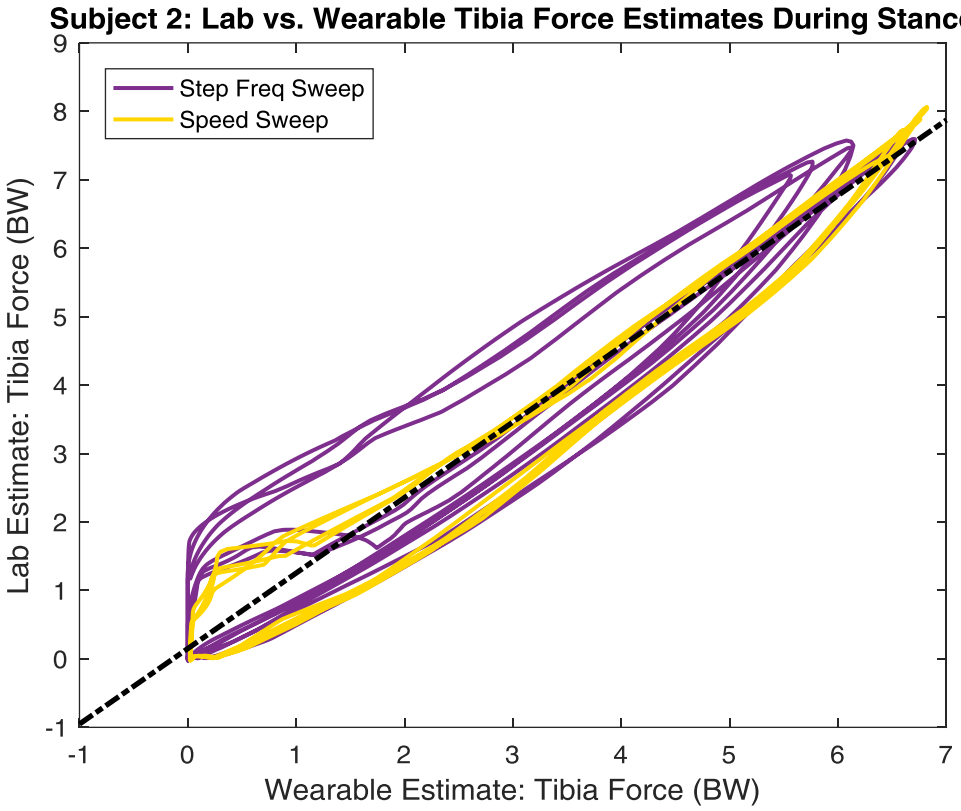

Figure 13. Lab estimates of tibia force versus wearable estimates of tibia force during stance for all trials completed by Subject 2 with a linear trendline fitted to the data.

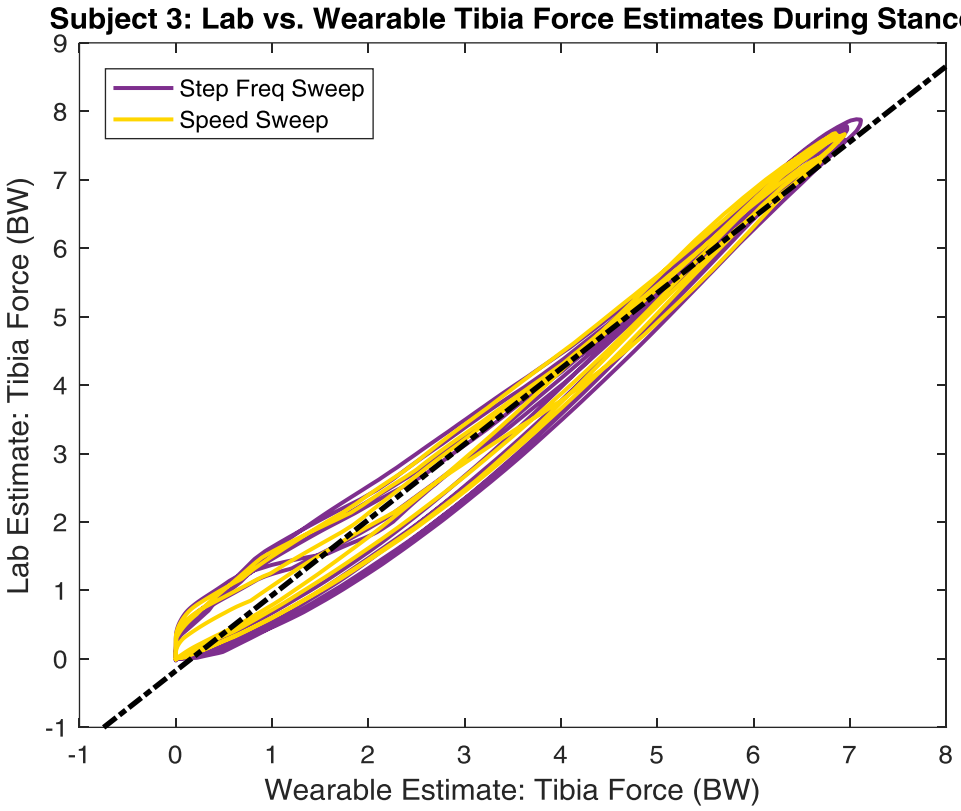

Figure 14. Lab estimates of tibia force versus wearable estimates of tibia force during stance for all trials completed by Subject 3 with a linear trendline fitted to the data.

While it may be possible to calibrate a wearable device for each user, it would be ideal if a single equation could be found to equate lab and wearable estimates of tibia load. As such, data for all three subjects in the study were combined, and an overall line of best fit was obtained. A plot of this data (with subjects shown in different colors) and the best fit line is shown in Figure 15. The best fit line yielded a root mean square error of 0.49 body weights (6.1% of max).

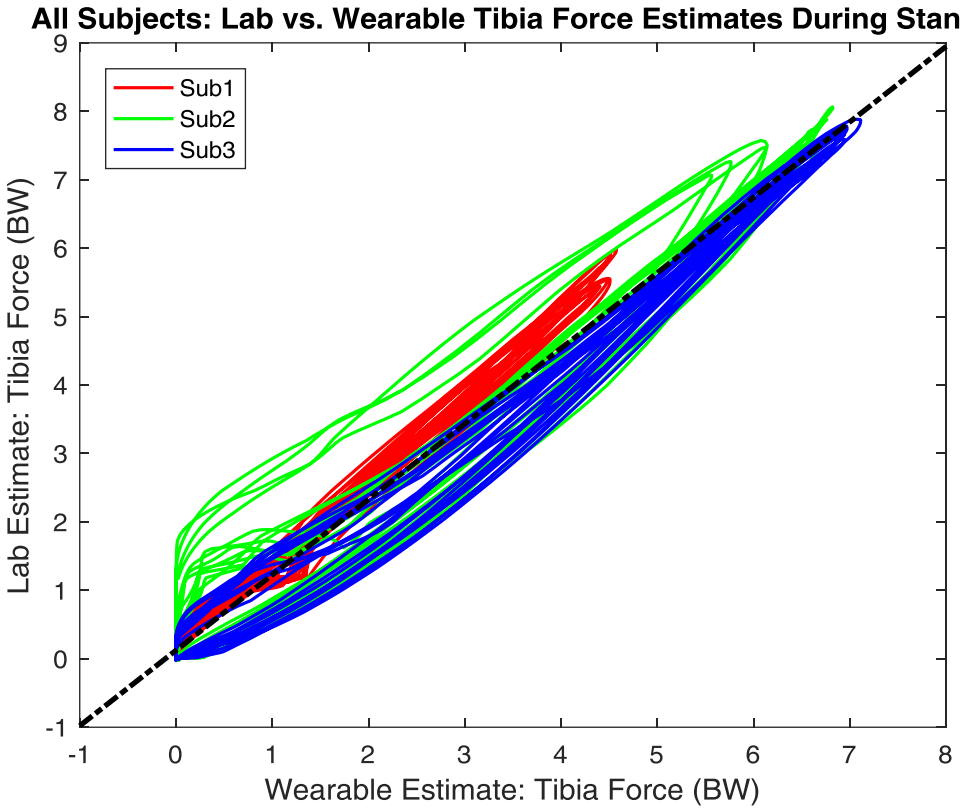

Figure 15. Lab estimates of tibia force versus wearable estimates of tibia force during stance for all trials completed by all subjects with a linear trendline fitted to the data.

Section 3.4 Wearable Estimates of Peak Tibia Force

Ideally, we want to be able to accurately estimate the tibia load throughout the entire stance phase, but this may not always be necessary; it may be that stress fracture development is impacted mainly by the peak forces experienced by the tibia, in which case, only peak forces would need to be accurately estimated. In this section, we analyze the accuracy of raw and calibrated peak tibia forces.

Section 3.4.1 Raw Estimates

Similar to the first test of accuracy for tibia force over stance, the root mean square error between lab based and raw wearable estimates of peak bone loading during stance was calculated for each subject and for all data combined. Results are included in Table 8. Subject 1 had a root mean square error in peak loading of 1.14 body weights (19.0% of max). Subject 2 had a root mean square error in peak loading of 1.18 body weights (14.6% of max). Subject 3 had a root mean square error in peak loading of 0.71 body weights (9.0% of max).

Section 3.4.2 Calibrated Estimates

Plots of lab estimates of peak tibia force vs wearable estimates of peak tibia force are included in Figures 16-18. A summary of results is shown in Table 8.

Table 8. Root mean square error in calibrated wearable estimates of peak tibia force for each subject.

	Subject 1	**Subject 2**	**Subject 3**
R^2	0.91	0.66	0.96
RMSE (BW)	0.15	0.16	0.08
RMSE (% Max)	2.5%	2.0%	1.0%

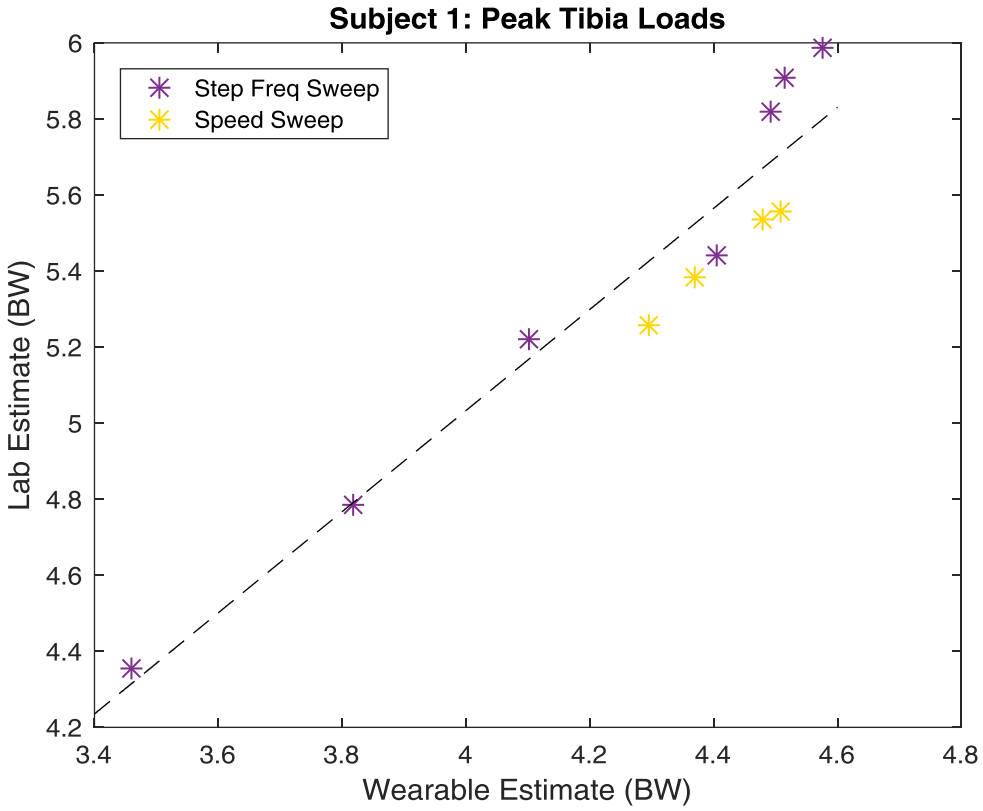

Figure 16. Lab estimates of peak tibia force plotted against wearable estimates for Subject 1, with a linear trendline fitted to the data.

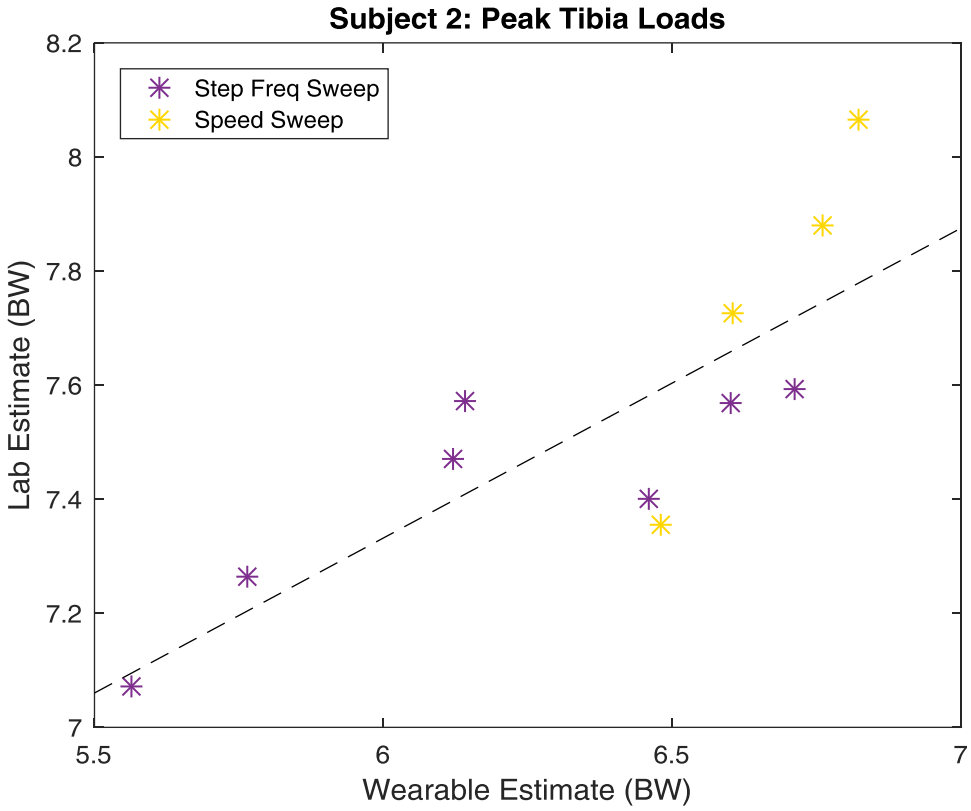

Figure 17. Lab estimates of peak tibia force plotted against wearable estimates for Subject 2, with a linear trendline fitted to the data.

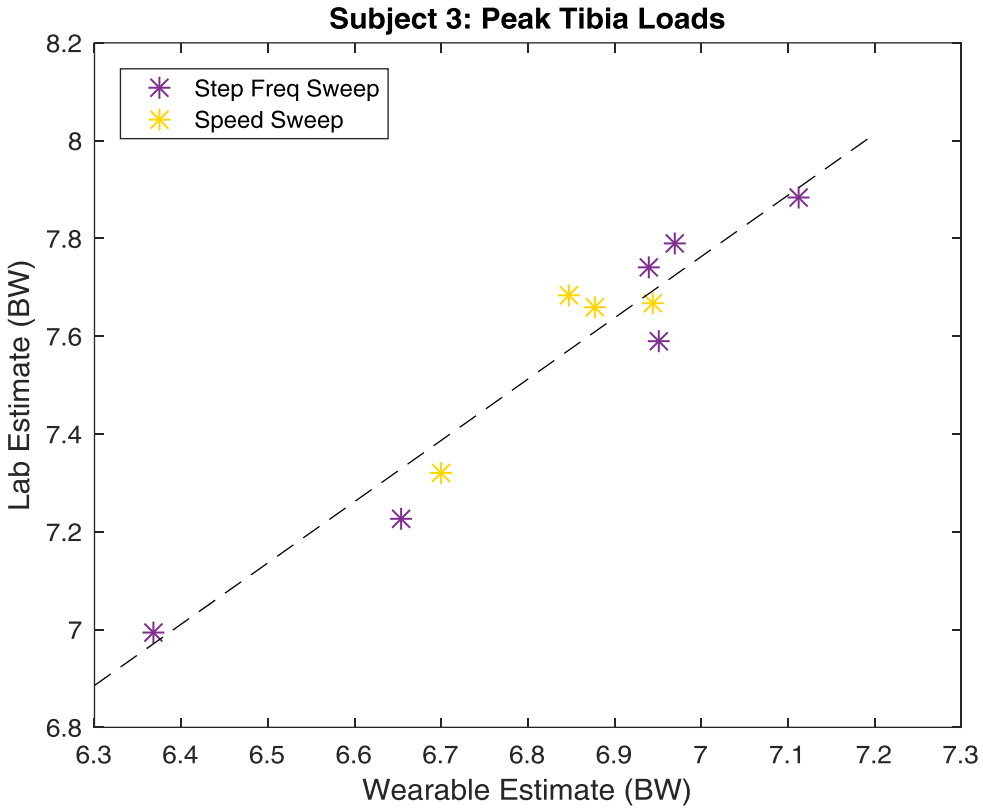

Figure 18. Lab estimates of peak tibia force plotted against wearable estimates for Subject 3, with a linear trendline fitted to the data.

A line of best fit was also found for the set of data for all subjects. The plot of lab estimates of peak tibia force versus wearable estimate of peak tibia force is shown in Figure 19. This overall best fit line is strongly correlated with an r-squared value of 0.95, and has a root mean square error of 0.25 body weights (3.1% of max).

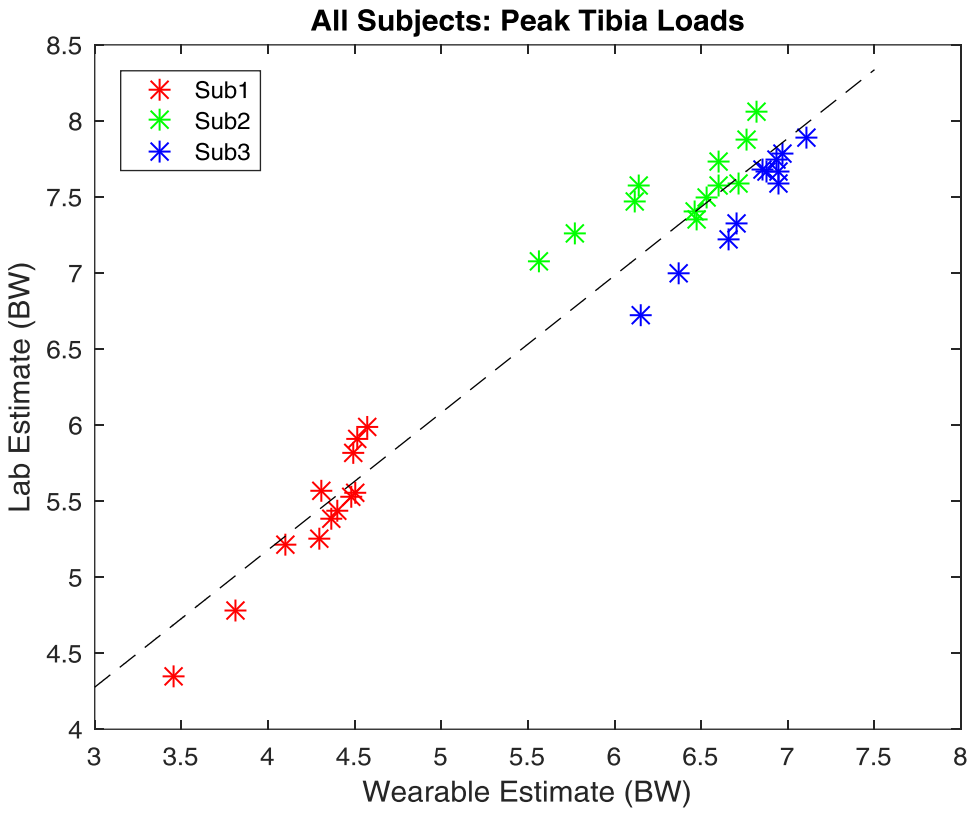

Figure 19. Lab estimates of peak tibia force plotted against wearable estimates for all subjects, with a linear trendline fitted to the data.

Section 3.5 Wearable Estimates of Tibia Load per Kilometer

In addition to peak tibia force, tibia load per kilometer has been identified as a metric that may help to quantify the cumulative effects of tibia bone loading cycles, so wearable estimates of this metric will also be analyzed.

Section 3.5.1 Raw Estimates

Following the same procedure as for tibia force during stance and peak tibia force, root mean square error between lab and raw wearable estimates of tibia load per kilometer was calculated for each subject and for all data combined. Subject 1 had a root mean square error in load per kilometer of 193.5 body weights times seconds (20.6% of max). Subject 2 had a root mean square error in load per kilometer of 136.7 body weights times seconds (13.4% of max). Subject 3 had a root mean square error in load per kilometer of 45.0 body weights times seconds (4.6% of max).

Section 3.5.2 Calibrated Estimates

Plots of lab estimates of tibia load per kilometer vs wearable estimates of tibia load per kilometer are included in Figures 20-22. Tibia load per kilometer tended to be underestimated by wearable sensors, and data points for the speed sweep trials tended to follow a more linear pattern than the step frequency sweep data points. A summary of results is included in Table 9.

Table 9. Root mean square error in calibrated wearable estimates of tibia load per kilometer for each subject.

	Subject 1	**Subject 2**	**Subject 3**
R^2	0.85	0.18	0.95
RMSE (BW*sec)	16.64	25.65	7.42
RMSE (% Max)	2.9%	4.1%	1.2%

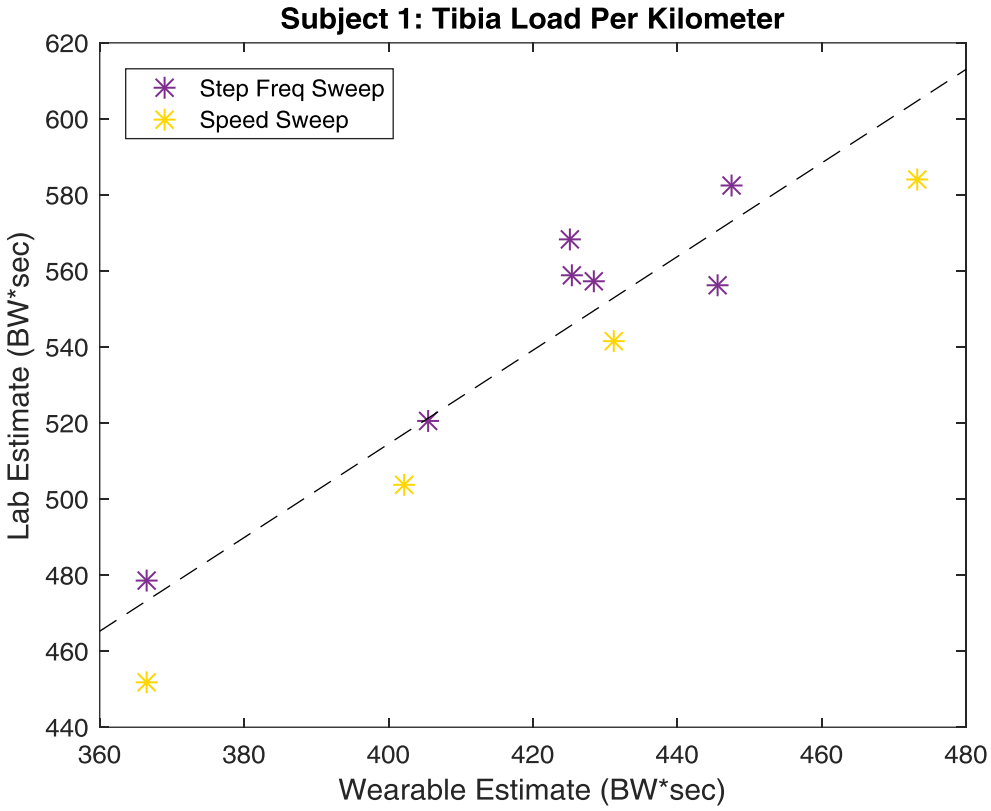

Figure 20. Lab estimates of tibia load per kilometer plotted against wearable estimates for Subject 1, with a linear trendline fitted to the data.

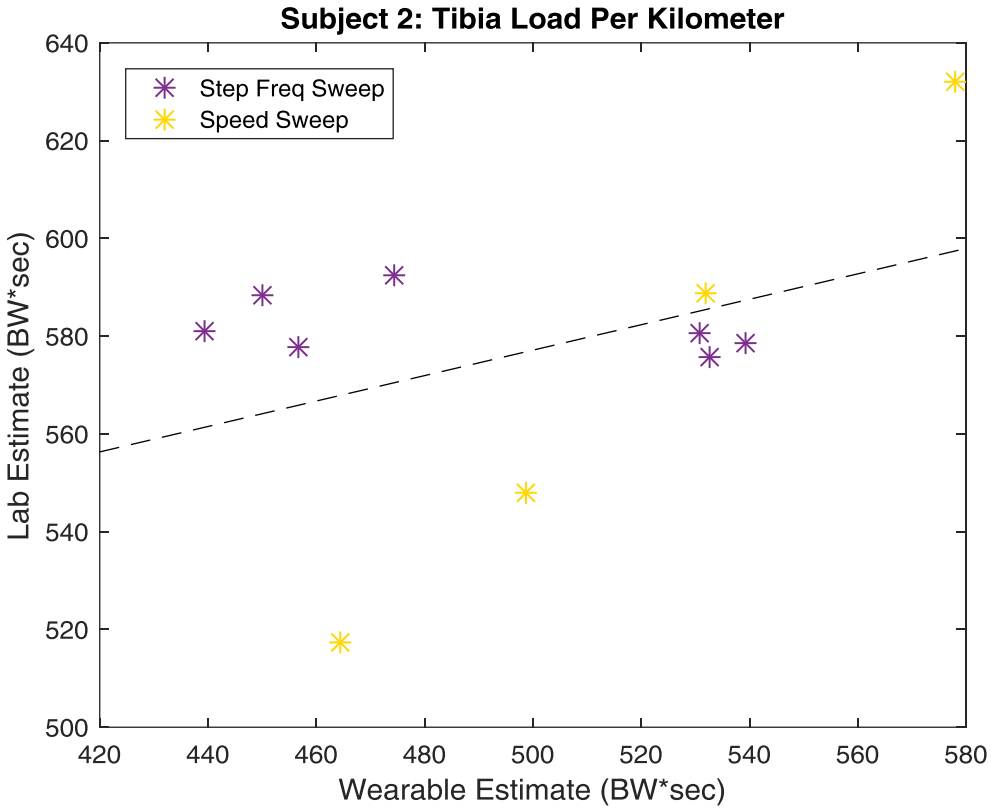

Figure 21. Lab estimates of tibia load per kilometer plotted against wearable estimates for Subject 2, with a linear trendline fitted to the data.

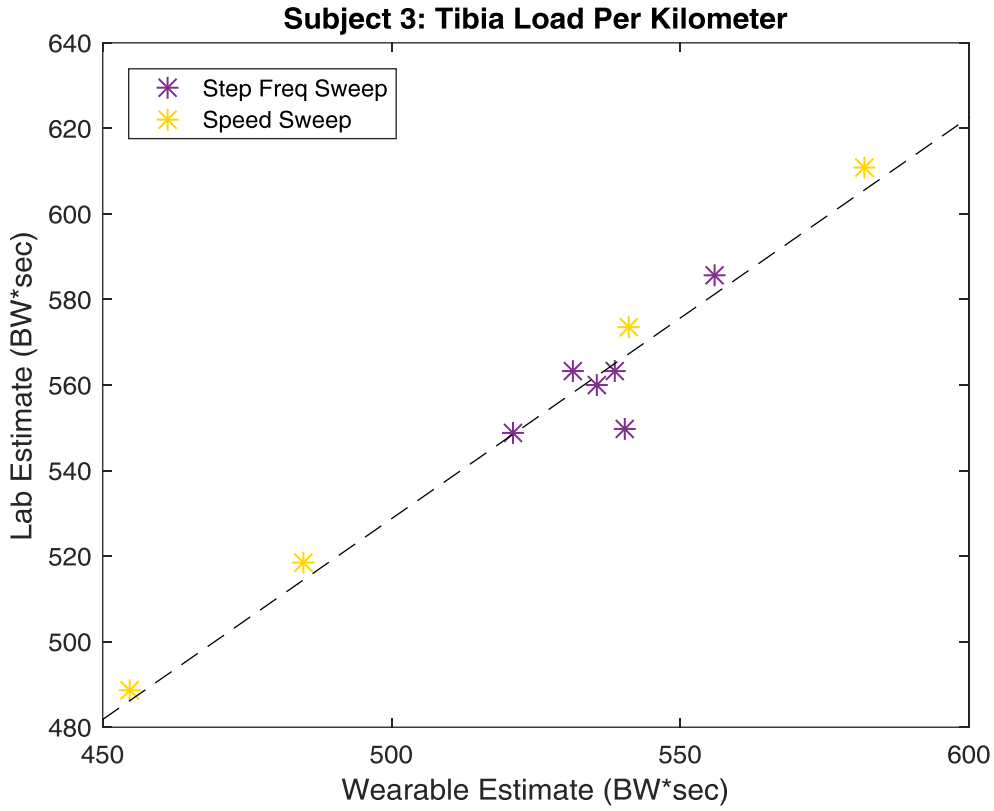

Figure 22. Lab estimates of tibia load per kilometer plotted against wearable estimates for Subject 3, with a linear trendline fitted to the data.

A line of best fit was also found for the set of data for all subjects. The plot of lab estimates of tibia load per kilometer versus wearable estimate of tibia load per kilometer is shown in Figure 23. This overall best fit line is somewhat correlated with an r-squared value of 0.40, and has a root mean square error of 29.3 body weights times seconds (4.6% of max).

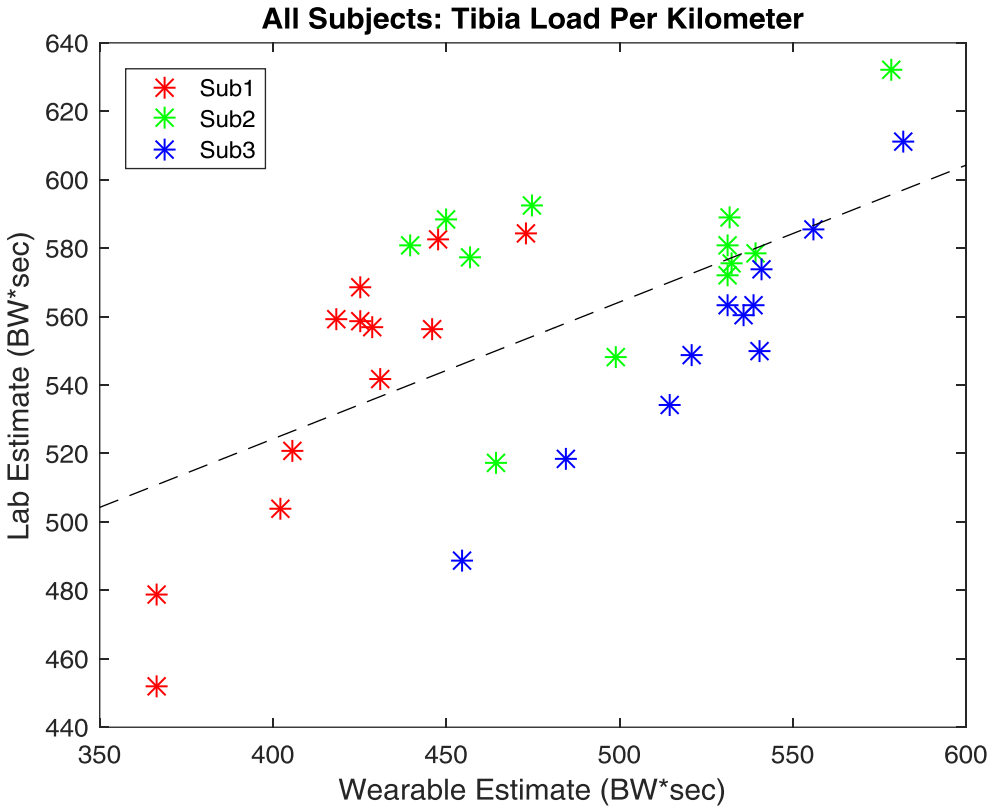

Figure 23. Lab estimates of tibia load per kilometer plotted against wearable estimates for all subjects, with a linear trendline fitted to the data.

Chapter 4: Discussion

Section 4.1 Evaluation of Accuracy

The initial hypothesis that the wearable estimate of tibia bone loading would be within a 10 percent root mean square error of the lab estimates is supported by the data obtained in this study. When calibrated with a scaling factor and constant offset (determined from a best fit line) on a subject by subject basis, accuracies between 3.0 and 7.7% for force across the entire stance phase, 1.0 and 2.5% for peak force, and 1.2 and 4.1% for load per kilometer were achieved. With a single calibration for all subjects, accuracies of 6.1% for force across the entire stance phase, 3.1% for peak force, and 4.6% for load per kilometer were achieved. For a relatively simple estimation method and small number of sensors (pressure insoles and a single IMU), these results are highly promising.

Section 4.2 Limitations

The current study analyzes a set of data averaged over a 20 second trial for each condition. While this is useful as a proof of concept for utilizing wearable sensors as surrogates for lab measurements in the calculation of tibia load, it is ultimately desired to have a device that can record data for all strides, not just an average. With so many open questions related to stress fracture development, we wish to develop a wearable device to measure bone loading that can collect as much accurate data as possible to analyze. Individual steps with high tibia loads or loading rates may be particularly interesting to investigate and should therefore be validated in a similar manner to this study. Specifically, the best fit lines found to correct wearable estimates of

tibia load to more closely match lab estimates may work on an average cycle but may not be as accurate on individual cycles. It remains to be determined whether a single calibration (either for a single subject or overall) would result in accurate estimates of step to step changes in bone loading within a single condition as well as across conditions. Furthermore, although results of using a single calibration for all subjects appears promising in these results, it should be noted that only three subjects were added, so errors may increase with the inclusion of more subjects, and subject specific calibrations may become necessary to achieve the desired range of accuracy in wearable estimates of tibia loads.

Section 4.3 Areas for Improvement

Aside from correcting wearable estimates for scaling and offset errors, there are many possible ways that estimates could be improved. First, better calibration and placement of sensors could help to improve accuracy of individual measurements such as force from pressure insoles or shank angle from an IMU. Along the same lines, the development of more accurate sensors could help to reduce the error in tibia force estimates. Other methods of compensating for lower quality data from wearable sensors, such as the one dimensional ground reaction force instead of the true three dimensional vector, may be investigated. For example, it may be possible to assume a given angle trajectory of the ground reaction force, which could be used in conjunction with the IMU shank angle to get a more accurate projection of ground reaction force onto the tibia. Beyond improving individual sensor data, a more complex estimation method could be implemented, taking into account portions of bone loading that were neglected in this study, such as contributions of foot inertia, ligaments, or co-contracting muscles, or variable moment arm of the muscles producing forces on the bone. It may also become apparent that

simple substitutions of data into the inverse dynamics equation does not yield results that are accurate enough for applications in injury prevention, so more sophisticated data processing, including machine learning, could be implemented to design a more accurate data fusion algorithm.

Section 4.4 Implementation

While an experiment in a laboratory setting is necessary for a study such as this, whose objective is to determine the accuracy of an estimation method, these results represent many ideal conditions that may not be present in everyday conditions in which an ultimate product would be used. For example, sensor placement would likely not be as secure or well calibrated by a user when compared to a trained researcher. This could result in inaccurate measurements or noise in the data due to movement of the physical sensors. Additionally, should the algorithm proposed in this study be implemented in a consumer device, there would be several limiting factors that may reduce the capabilities of the device or individual sensors, including cost, size, power and battery life, form factor or aesthetic, and durability. Furthermore, all calculations and analysis in this study were done in post-processing, whereas in a consumer device, it would likely be desirable to perform these calculations in real time. Therefore, the device would need to integrate a processing system and programming would need to be done ahead of time. While not necessarily impossible, these limitations would make it difficult to exactly replicate the accuracy of wearable estimates in a real device.

Section 4.5 Alternate Estimation Method: Regression Equation

The benefit of fusing wearable sensor data to estimate tibia bone loading is that it aims to track the source of loading that can cause stress fractures. Nevertheless, for certain ranges of running speed, step frequency, and/or varying terrains, there may also be other metrics which are less directly or causally related to bone stress fracture risk that might also provide a correlated surrogate estimate of loading. For instance, a simple regression equation combining speed and step frequency might provide useful information about tibia bone loading over some range of running conditions. However, it is important to recognize that such spatiotemporal metrics have no direct connection to the physical forces on the bone, the ultimate cause of stress fractures. Therefore, if runners adjust their technique as they become fatigued, or run differently from one run to another, a fixed relationship between bone load and spatiotemporal parameters may not exist.

Section 4.6 Desired Accuracy of Estimates

It remains to be determined just how accurate a device would need to be to detect whether or not a user is at risk of developing a stress fracture injury, but in order to find the required accuracy, an algorithm must first be developed. It is reasonable to believe that errors of 0.01 body weights or less would have little impact on determining stress fracture injury risk, given that peak loading of the bone is between 4 and 8 body weights. On the other hand, we know that errors of 10 body weights or more would be unacceptable since this would mean that peak loading could be estimated as zero or negative. Accuracy within one tenth to one body weight, as achieved in this experiment, may be acceptable, but after the testing of a device, it

may be determined that a higher accuracy is necessary to detect the magnitude of changes to bone loading associated with stress fracture development.

Section 4.7 Future Work

Step frequency and speed represent two running metrics that may change from run to run or over the course of a training regimen. However, these are not the only factors that may change, and are not the only variations in running that result in changes in bone loading. For example, running on up or down an incline will result in different forces felt by the tibia than running on level ground, but these conditions were not investigated in this study. Similarly, all trials in this experiment were performed on a smooth treadmill surface, but runners often experience rugged and varying terrains on everyday runs, and the resulting changes to bone loading were not determined in this study. These additional factors may influence the accuracy of wearable sensors, so future work in this area includes investigating how these factors and others contribute to bone loading, and how the proposed tibia force estimation method performs in these conditions.

Chapter 5: Conclusions

Tibia stress fractures are a prevalent injury in recreational runners, military recruits, and other active populations, yet little is known about the root causes of injury or how to identify potential risk factors prior to the onset of symptoms. Substantial progress has been made in the field of wearable technology for health and fitness monitoring in the last decade, and interest in these devices is high. Given the advances in sensors and data analytics, it may be possible to design a device that can measure tibia bone loading and help researchers determine indicators of stress fracture development, and ultimately alert users of potential injury risks. The goal of this study was to determine whether wearable sensor data could be used in an inverse dynamics-based method of calculating tibia force, an adaptation of the methods commonly used in a laboratory setting, to obtain accurate tibia force curves for running trials. While the level of accuracy required is not well-established, the initial goal was to obtain estimates within 10% root mean square error of lab estimates. Using the inverse dynamics approach with calibration, root mean square errors of 6.1% of peak force across the entire stance phase of running were obtained. This level of accuracy, particularly for a preliminary test of a relatively simple algorithm, is extremely promising, and motivates future work in this area. Once further testing and validation is completed, this method of calculating tibia bone loading in a portable system could help to improve our fundamental understanding of stress fracture injury and may even have applications in studying and detecting other musculoskeletal loading injuries.

References

Almonroeder, T., Willson, J. D., & Kernozek, T. W. (2013). The Effect of Foot Strike Pattern on Achilles Tendon Load During Running. *Annals of Biomedical Engineering*, *41*(8), 1758–1766. https://doi.org/10.1007/s10439-013-0819-1

Bennell, K., Matheson, G., Meeuwisse, W., & Brukner, P. (1999). Risk Factors for Stress Fractures. *Sports Medicine*, *28*(2), 91–122. https://doi.org/10.2165/00007256-199928020-00004

Biewener, A. A., & Taylor, C. R. (1986). Bone strain: a determinant of gait and speed? *Journal of Experimental Biology*, *123*(1), 383–400.

Bogey, R. A., Perry, J., & Gitter, A. J. (2005). An EMG-to-force processing approach for determining ankle muscle forces during normal human gait. *IEEE Transactions on Neural Systems and Rehabilitation Engineering*, *13*(3), 302–310. https://doi.org/10.1109/TNSRE.2005.851768

Diehl, J. J., Best, T. M., & Kaeding, C. C. (2006). Classification and Return-to-Play Considerations for Stress Fractures. *Clinics in Sports Medicine*, *25*(1), 17–28. https://doi.org/10.1016/j.csm.2005.08.012

D'Lima, D. D., Patil, S., Steklov, N., Slamin, J. E., & Colwell, C. W. (2006). Tibial Forces Measured In Vivo After Total Knee Arthroplasty. *The Journal of Arthroplasty*, *21*(2), 255–262. https://doi.org/10.1016/j.arth.2005.07.011

Edwards, W. B., Taylor, D., Rudolphi, T., Gillette, J., & Derrick, T. (2009). Effects of Stride Length and Running Mileage on a Probabilistic Stress Fracture Model. *Medicine & Science in Sports & Exercise*, 2177–2184. https://doi.org/10.1249/MSS.0b013e3181a984c4

Edwards, W. B., Taylor, D., Rudolphi, T. J., Gillette, J. C., & Derrick, T. R. (2010). Effects of running speed on a probabilistic stress fracture model. *Clinical Biomechanics*, *25*(4), 372–377. https://doi.org/10.1016/j.clinbiomech.2010.01.001

Eng, J. J., & Winter, D. A. (1995). Kinetic analysis of the lower limbs during walking: What information can be gained from a three-dimensional model? *Journal of Biomechanics*, *28*(6), 753–758. https://doi.org/10.1016/0021-9290(94)00124-M

Farley, C. T., & González, O. (1996). Leg stiffness and stride frequency in human running. *Journal of Biomechanics*, *29*(2), 181–186. https://doi.org/10.1016/0021-9290(95)00029-1

Funk, J. R., Rudd, R. W., Kerrigan, J. R., & Crandall, J. R. (2004). The effect of tibial curvature and fibular loading on the tibia index. *Traffic Injury Prevention*, *5*(2), 164–172. https://doi.org/10.1080/15389580490436069

Ghiasi, M. S., Chen, J., Vaziri, A., Rodriguez, E. K., & Nazarian, A. (2017). Bone fracture healing in mechanobiological modeling: A review of principles and methods. *Bone Reports*, *6*, 87–100. https://doi.org/10.1016/j.bonr.2017.03.002

Goldberg, B., & Pecora, C. (1994). Stress Fractures. *The Physician and Sportsmedicine*, *22*(3), 68–78. https://doi.org/10.1080/00913847.1994.11710482

Harrast, M. A., & Colonno, D. (2010). Stress Fractures in Runners. *Clinics in Sports Medicine*, *29*(3), 399–416. https://doi.org/10.1016/j.csm.2010.03.001

Heiderscheit, B. C., Chumanov, E. S., Michalski, M. P., Wille, C. M., & Ryan, M. B. (2011). Effects of Step Rate Manipulation on Joint Mechanics during Running. *Medicine and Science in Sports and Exercise*, *43*(2), 296–302. https://doi.org/10.1249/MSS.0b013e3181ebedf4

Hobara, H., Sato, T., Sakaguchi, M., Sato, T., & Nakazawa, K. (2012). Step Frequency and Lower Extremity Loading During Running. *International Journal of Sports Medicine*, *33*(04), 310–313. https://doi.org/10.1055/s-0031-1291232

Honert, E. C., & Zelik, K. E. (2016). Inferring Muscle-Tendon Unit Power from Ankle Joint Power during the Push-Off Phase of Human Walking: Insights from a Multiarticular EMG-Driven Model. *PLOS ONE*, *11*(10), e0163169. https://doi.org/10.1371/journal.pone.0163169

Kaufman, K. R., Kovacevic, N., Irby, S. E., & Colwell, C. W. (1996). Instrumented implant for measuring tibiofemoral forces. *Journal of Biomechanics*, *29*(5), 667–671. https://doi.org/10.1016/0021-9290(95)00124-7

Kernozek, T., Gheidi, N., & Ragan, R. (2017). Comparison of estimates of Achilles tendon loading from inverse dynamics and inverse dynamics-based static optimisation during running. *Journal of Sports Sciences*, *35*(21), 2073–2079. https://doi.org/10.1080/02640414.2016.1255769

Lambert, K. L. (1971). The weight-bearing function of the fibula. A strain gauge study. *The Journal of Bone and Joint Surgery. American Volume*, *53*(3), 507–513.

Lanyon, L. E., Hampson, W. G. J., Goodship, A. E., & Shah, J. S. (1975). Bone Deformation Recorded in vivo from Strain Gauges Attached to the Human Tibial Shaft. *Acta Orthopaedica Scandinavica*, *46*(2), 256–268. https://doi.org/10.3109/17453677508989216

Maganaris, C. N., Baltzopoulos, V., & Sargeant, A. J. (1998). Changes in Achilles tendon moment arm from rest to maximum isometric plantarflexion: in vivo observations in man. *The Journal of Physiology*, *510*(Pt 3), 977–985. https://doi.org/10.1111/j.1469-7793.1998.977bj.x

Martin, R. B., Burr, D. B., Sharkey, N. A., & Fyhrie, D. P. (2015). *Skeletal Tissue Mechanics*. Springer.

Matheson, G. O., Clement, D. B., Mckenzie, D. C., Taunton, J. E., Lloyd-Smith, D. R., & Macintyre, J. G. (1987). Stress fractures in athletes: A study of 320 cases. *The American Journal of Sports Medicine*, *15*(1), 46–58. https://doi.org/10.1177/036354658701500107

McCullough, M. B. A., Ringleb, S. I., Arai, K., Kitaoka, H. B., & Kaufman, K. R. (2011). Moment Arms of the Ankle Throughout the Range of Motion in Three Planes. *Foot & Ankle International*, *32*(3), 300–306. https://doi.org/10.3113/FAI.2011.0300

Milgrom, C., Giladi, M., Stein, M., Kashtan, H., Margulies, J., Chisin, R., … Aharonson, Z. (1985). Stress fractures in military recruits. A prospective study showing an unusually high incidence. *The Journal of Bone and Joint Surgery. British Volume*, *67-B*(5), 732–735. https://doi.org/10.1302/0301-620X.67B5.4055871

Miller, R. H., Esterson, A. Y., & Shim, J. K. (2015). Joint contact forces when minimizing the external knee adduction moment by gait modification: A computer simulation study. *The Knee*, *22*(6), 481–489. https://doi.org/10.1016/j.knee.2015.06.014

Milner, C. E., Ferber, R., Pollard, C. D., Hamill, J., & Davis, I. S. (2006). Biomechanical factors associated with tibial stress fracture in female runners. *Medicine and Science in Sports and Exercise*, *38*(2), 323–328. https://doi.org/10.1249/01.mss.0000183477.75808.92

Moissenet, F., Chèze, L., & Dumas, R. (2014). A 3D lower limb musculoskeletal model for simultaneous estimation of musculo-tendon, joint contact, ligament and bone forces during gait. *Journal of Biomechanics*, *47*(1), 50–58. https://doi.org/10.1016/j.jbiomech.2013.10.015

Morin, J. B., Samozino, P., Zameziati, K., & Belli, A. (2007). Effects of altered stride frequency and contact time on leg-spring behavior in human running. *Journal of Biomechanics*, *40*(15), 3341–3348. https://doi.org/10.1016/j.jbiomech.2007.05.001

Morrison, J. B. (1970). The mechanics of the knee joint in relation to normal walking. *Journal of Biomechanics*, *3*(1), 51–61. https://doi.org/10.1016/0021-9290(70)90050-3

Mündermann, A., Dyrby, C. O., D'Lima, D. D., Colwell, C. W., & Andriacchi, T. P. (2008). In vivo knee loading characteristics during activities of daily living as measured by an instrumented total knee replacement. *Journal of Orthopaedic Research*, *26*(9), 1167–1172. https://doi.org/10.1002/jor.20655

Nigg, B. (2010). *Biomechanics of sport shoes*. University of Calgary.

Nigg, B., Mohr, M., & Nigg, S. R. (2017). Muscle tuning and preferred movement path - a paradigm shift. *Current Issues in Sport Science (CISS)*, *0*(0). Retrieved from https://webapp.uibk.ac.at/ojs2/index.php/ciss/article/view/2391

Orava, S., & Hulkko, A. (1984). Stress fracture of the mid-tibial shaft. *Acta Orthopaedica Scandinavica*, *55*(1), 35–37. https://doi.org/10.3109/17453678408992308

Robertson, G., Caldwell, G., Hamill, J., Kamen, G., & Whittlesey, S. (2013). *Research Methods in Biomechanics, 2E*. Human Kinetics.

Rugg, S. G., Gregor, R. J., Mandelbaum, B. R., & Chiu, L. (1990). In vivo moment arm calculations at the ankle using magnetic resonance imaging (MRI). *Journal of Biomechanics*, *23*(5), 495–497. https://doi.org/10.1016/0021-9290(90)90305-M

Sasimontonkul, S., Bay, B. K., & Pavol, M. J. (2007). Bone contact forces on the distal tibia during the stance phase of running. *Journal of Biomechanics*, *40*(15), 3503–3509. https://doi.org/10.1016/j.jbiomech.2007.05.024

Schubert, A. G., Kempf, J., & Heiderscheit, B. C. (2014). Influence of Stride Frequency and Length on Running Mechanics: A Systematic Review. *Sports Health*, *6*(3), 210–217. https://doi.org/10.1177/1941738113508544

Scott, S. H., & Winter, D. A. (1990). Internal forces of chronic running injury sites. *Medicine and Science in Sports and Exercise*, *22*(3), 357–369.

Sharkey, N. A., & Hamel, A. J. (1998). A dynamic cadaver model of the stance phase of gait: performance characteristics and kinetic validation. *Clinical Biomechanics*, *13*(6), 420–433. https://doi.org/10.1016/S0268-0033(98)00003-5

Siegler, S., Moskowitz, G. D., & Freedman, W. (1984). Passive and active components of the internal moment developed about the ankle joint during human ambulation. *Journal of Biomechanics*, *17*(9), 647–652. https://doi.org/10.1016/0021-9290(84)90118-0

Silder, A., Heiderscheit, B., & Thelen, D. G. (2008). Active and passive contributions to joint kinetics during walking in older adults. *Journal of Biomechanics*, *41*(7), 1520–1527. https://doi.org/10.1016/j.jbiomech.2008.02.016

Silder, A., Whittington, B., Heiderscheit, B., & Thelen, D. G. (2007). Identification of passive elastic joint moment–angle relationships in the lower extremity. *Journal of Biomechanics*, *40*(12), 2628–2635. https://doi.org/10.1016/j.jbiomech.2006.12.017

Steele, K. M., Demers, M. S., Schwartz, M. H., & Delp, S. L. (2012). Compressive tibiofemoral force during crouch gait. *Gait & Posture*, *35*(4), 556–560. https://doi.org/10.1016/j.gaitpost.2011.11.023

Taylor, S. J. G., Walker, P. S., Perry, J. S., Cannon, S. R., & Woledge, R. (1998). The forces in the distal femur and the knee during walking and other activities measured by telemetry. *The Journal of Arthroplasty*, *13*(4), 428–437. https://doi.org/10.1016/S0883-5403(98)90009-2

Thambyah, A., Pereira, B. P., & Wyss, U. (2005). Estimation of bone-on-bone contact forces in the tibiofemoral joint during walking. *The Knee*, *12*(5), 383–388. https://doi.org/10.1016/j.knee.2004.12.005

Winter, D. A. (2009). *Biomechanics and Motor Control of Human Movement*. John Wiley & Sons.

Worp, H. van der, Vrielink, J. W., & Bredeweg, S. W. (2016). Do runners who suffer injuries have higher vertical ground reaction forces than those who remain injury-free? A systematic review and meta-analysis. *Br J Sports Med*, *50*(8), 450–457. https://doi.org/10.1136/bjsports-2015-094924

Yang, P.-F., Sanno, M., Ganse, B., Koy, T., Brüggemann, G.-P., Müller, L. P., & Rittweger, J. (2014). Torsion and Antero-Posterior Bending in the In Vivo Human Tibia Loading Regimes during Walking and Running. *PLOS ONE*, *9*(4), e94525. https://doi.org/10.1371/journal.pone.0094525

Appendix

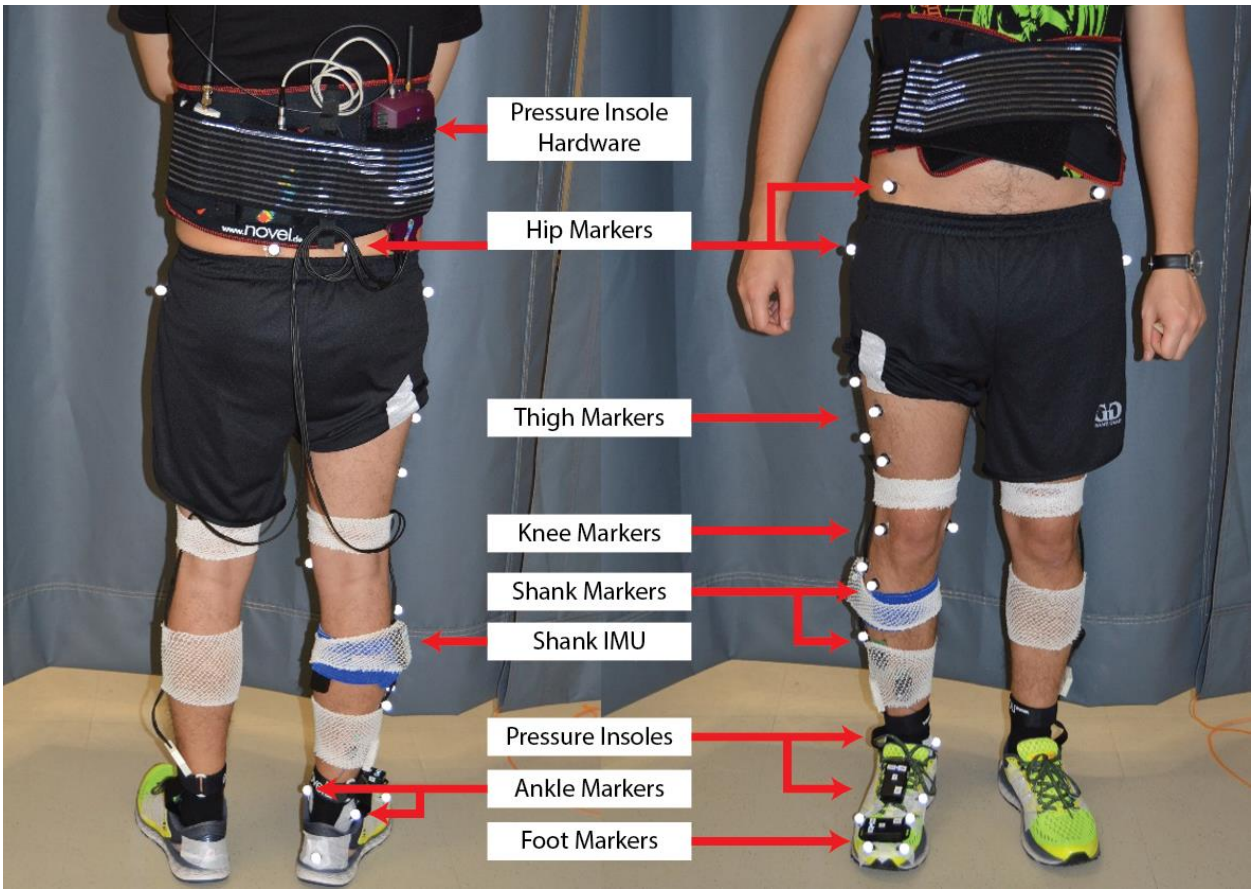
Pressure Insole Hardware
Hip Markers
Thigh Markers
Knee Markers
Shank Markers
Shank IMU
Pressure Insoles
Ankle Markers
Foot Markers